Regional-scale transport of air pollutants: Impacts of southern California emissions on Phoenix ground-level ozone concentrations

J. Li[1*], M. Georgescu[1,2,], P. Hyde[3], A. Mahalov[1], and M. Moustaoui[1]

[1] Julie Ann Wrigley Global Institute of Sustainability, School of Mathematical and Statistical Sciences, Arizona State University, Tempe, AZ 85287, USA

[2] School of Geographical Sciences and Urban Planning, Arizona State University, Tempe, AZ 85287, USA

[3] School for Engineering of Matter, Transport and Energy, Arizona State University, Tempe, AZ 85287, USA

[*]**Corresponding Author**: Jialun.Li@asu.edu

Revised manuscript submitted to *Atmospheric Chemistry and Physics*

August, 2015

Abstract

In this study, WRF-Chem is utilized at high-resolution (1.333-km grid spacing for the innermost domain) to investigate impacts of southern California anthropogenic emissions (SoCal) on Phoenix ground-level ozone concentrations ($[O_3]$) for a pair of recent exceedance episodes. First, WRF-Chem control simulations, based on the U.S. Environmental Protection Agency (EPA) 2005 National Emissions Inventories (NEI05), are conducted to evaluate model performance. Compared with surface observations of hourly ozone, CO, NO_X, and wind fields, the control simulations reproduce observed variability well. Simulated $[O_3]$ are comparable with the previous studies in this region. Next, the relative contribution of SoCal and Arizona local anthropogenic emissions (AZ) to ozone exceedances within the Phoenix metropolitan area is investigated via a trio of sensitivity simulations: (1) SoCal emissions are excluded, with all other emissions as in Control; (2) AZ emissions are excluded with all other emissions as in Control; and (3) SoCal and AZ emissions are excluded (i.e., all anthropogenic emissions are eliminated) to account only for BIogenic emissions and lateral boundary inflow(BILB). Based on the USEPA NEI05, results for the selected events indicate the impacts of AZ emissions are dominant on daily maximum 8 h average (DMA8) $[O_3]$ in Phoenix. SoCal contributions to DMA8 $[O_3]$ for the Phoenix metropolitan area range from a few ppbv to over 30 ppbv (10%-30% relative to Control experiments). $[O_3]$ from SoCal and AZ emissions exhibit the expected diurnal characteristics that are determined by physical and photochemical processes, while BILB contributions to DMA8 $[O_3]$ in Phoenix also play a key role.

Finally, ozone transport processes and pathways within the lower troposphere are investigated. During daytime, pollutants (mainly ozone) near the southern California coasts are

47 pumped into the planetary boundary-layer over the southern California desert through the
48 mountain chimney and pass channel effects, aiding eastward transport along the desert air basins
49 in southern California and finally, northeastward along the lower Gila River basin in Arizona,
50 thereby affecting Phoenix air quality during subsequent days. This study indicates that local
51 emission controls in Phoenix need to be augmented with regional emission reductions to attain
52 the federal ozone standard, especially if a more stringent standard is adopted in the future.

1. **Introduction**

Tropospheric ozone is a strong oxidant controlling much of the chemistry in the atmosphere, such as hydroxyl radical production and the lifetime of atmospheric species (see review in He et al., 2013). Tropospheric ozone is also a greenhouse gas and acts as an important anthropogenic contributor to radiative forcing of climate (IPCC, 2007). Lower tropospheric ozone adversely affects human health (Anderson, 2009; Smith et al., 2009), reduces crop yields (Avnery et al., 2011; Chameides et al., 1999), and damages natural ecosystems (Ashmore, 2005; Mauzeral and Wang, 2001). Therefore, ozone (O_3) is one of the six criteria pollutants regulated by the US Environmental Protection Agency (EPA) through National Ambient Air Quality Standards (NAAQS). The current NAAQS for O_3 concentrations ([O_3]) is 75 ppbv, defined as the 3-year average of the annual fourth-highest daily maximum 8 h average (DMA8) [O_3] for each monitoring site within an airshed. The US EPA has already proposed to lower the standard to 65-70 ppbv (EPA 2014) and may also redefine the national O_3 secondary standard for protecting sensitive vegetation and ecosystems (Huang et al., 2013). Currently, many U.S. cities are classified as NAAQS O_3 nonattainment areas based on the 2008 federal standard (http://www.epa.gov/airquality/greenbook/hnc.html). In addition, sensitive areas (e.g., national parks and wilderness areas) also experience DMA8 O_3 exceedances (http://www.nature.nps.gov/air/Monitoring/exceed.cfm). Therefore, improved understanding and attribution of [O_3] sources in these areas is necessary to develop effective air quality management strategies to achieve ever more stringent US air quality standards.

As a secondary pollutant, measured ground-level [O_3] is the result of O_3 production/loss due to local sources of precursor emissions, to transport of O_3 and its precursors from nearby

and/or remote regions, and to ozone formed from natural precursor emissions. The direct way to characterize O_3 source attribution is through field measurements (e.g., Fast et al., 2002; Kemball-Cook et al., 2009; Nunnermacker et al., 2004). The other way to identify transported O_3 and local generated O_3 is to use trajectory models (e.g., MacDonald et al., 2006; Lanford et al., 2010).

Transport of ozone and its precursors from one area to another is determined by flow patterns, which can be obtained by measurement and/or modeling. However, information on flow alone is insufficient in ozone studies because of the complexity of the chemistry involved, wherein ozone and precursors nonlinearly interact with flow, turbulence and sunlight to determine ozone distributions (Huang, et al., 2013; Lee et al., 2003; 2007; Levy II et al., 1985). Chemical transport models (CTMs) are increasingly common in simulating atmospheric chemical and transport processes at regional/continental/global scales because of the detailed physical and chemical processes which they're capable of simulating. For example, using a CTM (GFDL AM3), Lin et al. (2012) found that Asian O_3 pollutants can affect surface [O_3] in the western U.S., contributing up to 8-15 ppbv to the DMA8; and that Asian pollution increases the DMA8 O_3 exceedance days by 53% in the southwestern U.S. Huang et al. (2013), combining model simulations at 12-km resolution (WRF/STEM), remote-sensing, and ground-based observations, have studied the effect of southern California anthropogenic emissions (SoCal) on ozone pollution in southwestern U.S. mountain states. They found that the SoCal precursor emissions and its transported ozone increased [O_3] up to 15 ppbv in western Arizona. They also characterized the nonlinear relationship between emissions and [O_3]. However, these studies

96 have not examined the impacts of regional emissions on [O_3] in an urban setting (such as
97 Phoenix), at high-resolution.

98 Physical/chemical-based CTM modeling is the only available tool for ozone transport
99 predictions on finer spatial scales (Lee et al., 2007). Many studies have investigated ozone
100 transport at urban scales using coupled meteorological and chemistry models. For example, Lu
101 et al. (1997) found that ozone and other pollutant concentrations were higher in northern and
102 eastern Los Angeles (LA) than those in the western and central greater LA, where strong emission
103 sources are located, due to transport owing to the persistent onshore sea breeze and mountain-
104 induced upslope flow. Analogously, that surface [O_3] in the Phoenix metropolitan area and its
105 rural environs are higher in northeastern than in southwestern Phoenix arises from transport of
106 urban pollutants by prevailing southwest winds (Fast et al., 2000; Lee et al., 2003 , 2007; Lee and
107 Fernando, 2013). Although these studies have considered both chemistry and transport
108 processes at the urban scale, they did not try to distinguish between ozone produced by local
109 emissions and that produced by regional transport, a principal motivation of this study.

110 The Phoenix metropolitan area is classified as an O_3 nonattainment area under the 2008
111 NAAQS primary O_3 standard (http://www.epa.gov/airquality/greenbook/hnc.html). Therefore,
112 it is helpful to separately quantify the relative contributions of local emissions and regional
113 transport to Phoenix [O_3] in order to design feasible and effective ozone control strategies. Both
114 aircraft observations (Nunnermacker et al., 2004) and backward trajectory analysis (MacDonald
115 et al., 2006) indicate that surface [O_3] on exceedance days are attributed to both Arizona local
116 anthropogenic emissions (AZ) and regional and/or continental transport. Therefore, our focus
117 is to use a CTM to separately quantify the contributions of local and regional emissions to the

ozone distributions in Phoenix on exceedance days, research which has not been published in peer-reviewed journals.

In addition, previous studies indicate that coarse-resolution modeling cannot adequately represent the heterogeneities of ozone and meteorological fields in Phoenix due to its complex terrain (Fast et al., 2000; Lee et al., 2003; Lee and Fernando, 2013). That high-resolution CTMs can obtain better results in modeling urban air quality is also reported for the LA basin, Mexico City, and other regions (e.g., Tie et al., 2010; Chen at al., 2013; Lu and Turco, 1995; 1996; Taha, 2008; Klich and FueIberg, 2014; Stock et al., 2014). Therefore, employing a high-resolution CTM to address air pollutant distributions in the Phoenix metropolitan area due to local emissions and regional transport is our second motivation.

Using WRF-Chem (Grell et al., 2005) at high-resolution, we will examine: (1) the relative contributions of SoCal and AZ to the ozone episodes in Phoenix, and (2) how SoCal (emissions) affect Phoenix [O_3]. This is a topic that has received limited research attention to date (Moore, 2014), but requires investigation because of the metropolitan area's non-attainment ozone status and because of the need to evaluate the effectiveness of local anthropogenic emission control strategies necessary to attain the standard.

2. Methodology

2.1 WRF-Chem setup

We chose WRF-Chem (version 3.5.1) as the CTM since it has been successfully used in this region (Chen et al., 2011; Li et al., 2014; Zhao et al., 2012). In WRF-Chem, the Weather Research and Forecasting (WRF) model (Skamarock et al., 2008) is employed to resolve atmospheric

140 physics and dynamical processes, while the coupled chemistry (Chem) model is used to simulate
141 chemical processes such as gaseous and aqueous chemical reactions, dispersion, and deposition.
142 The WRF-Chem setup consists of the Lin's cloud scheme (Lin et al., 1983), the RRTM radiation
143 scheme (Mlawer et al., 1997), the Noah land surface model with single layer urban canopy model
144 (Chen and Dudhia, 2001; Chen et al., 2011; Ek et al., 2003), the Grell-Devenyi ensemble cumulus
145 scheme (Grell and Devenyi, 2002) that allows subsidence and spreading at high-resolution, a
146 revised MM5 surface layer, and the BouLac Planetary Boundary Layer (PBL) schemes. Land cover
147 and land use data from the MODIS 1-km resolution dataset (Friendl et al., 2002) are combined
148 with the 2006 National Land Cover Database (NLCD) 3-class urban covers to better represent the
149 urban landscape. The second generation regional acid deposition model (RADM2, Stockwell et
150 al., 1990; Gross and Stockwell, 2003) is used for gas-phase chemical reactions. The aerosol
151 algorithms are based on the MADE/SORGAM (Ackermann et al., 1998; Shell et al., 2001) with
152 GOCART, functioning as an emission scheme that accounts for surface wind speed, soil moisture,
153 and soil erodibility (Ginoux et al., 2001; Zhao et al., 2010). The other selected chemistry schemes
154 are based on the recommendations provided in the WRF-Chem users' guide (Peckam et al.,
155 2013).

156 Four nested domains are used (Figure 1a). The first (domain 1) has 36-km grid spacing and
157 covers the western and central U.S., eastern Pacific, northern and central Mexico, the Gulf of
158 California, and the western Gulf of Mexico. Nested domains 2, 3, and 4 use grid spacings of 12-
159 km, 4-km, and 1.333-km, respectively. The innermost domain (1.333-km) grid spacing (with 640
160 by 301 grid cells) encompasses southern California (the South Coast Air Basin or greater Los
161 Angeles Air Basin, the San Diego Air Basin, the southern Mojave Desert Air Basin, the Salton Sea

Air Basin, the southern part of the South Central Air Basin), and the central and southern Arizona airsheds to better represent the complex terrain and land cover features (see Figure 1b). As shown in Figure 1b, the mountainous features in southern California and Arizona are well represented at high resolution. The San Gorgonio Pass (between the San Bernardino Mountains and the San Jacinto Mountains), the Cajon Pass (between the San Gabriel Mountains and the San Bernardino Mountains), and the Newhall Pass (west of the San Gabriel Mountains) are also resolved. The vertical configuration of the model comprised 41 layers: the lowest 15 layers are within 1500 m a.g.l. and the first half-vertical layer above the land surface is at 12.5 m a.g.l. The observation sites (including O_3, NO_x, CO, and surface wind observations) used for validation of the control simulations are also superimposed (Fig. 1b).

2.2 Data used for model initialization and evaluation

The biogenic emission data are obtained from the 1-km resolution Model of Emissions of Gases and Aerosols from Nature (MEGAN, Guenther et al., 2006). The North American Regional Reanalysis (NARR; Mesinger et al., 2006) product is used for initial and boundary conditions (atmospheric and land surface [e.g., soil moisture and temperature]). NARR data are distributed on a 32-km grid with a 3-hour temporal frequency. The atmospheric chemical boundary and initial conditions are obtained from MOZART-4/GEOS-5 (http://www.acd.ucar.edu/wrf-chem/mozart.shtml) for 2012 case and MOZART-4/NCEP T42 for 2005 case (Emmons et al., 2010).

The anthropogenic emissions used in this study are obtained from 2005 National Emissions Inventories (NEI05) data provided by the U.S. EPA

(www.epa.gov/ttnchie1/net/2005inventory.html). These data are distributed on a 4-km grid array covering the U.S. and surrounding land areas. A method utilized to interpolate the 4-km grid spacing NEI05 data to any resolution one wishes to use for WRF-Chem simulations is provided with the WRF-Chem system (http://www.acd.ucar.edu/wrf-chem/). Each WRF-Chem model grid point data is based on averaging from those NEI05 grid points that fall within a distance less than the WRF-Chem model resolution. The method works well when WRF-Chem grid spacing is coarser than 4-km. However, the method misrepresents emissions when the model resolution is greater than the NEI05 grid. To overcome this issue, we have used Monotonic Cubic Interpolation to downscale the 4-km resolution NEI05 data to a 1.333-km resolution grid (the finest model grid spacing of our WRF-Chem simulations). Details on the NEI05 downscaling method and improved simulation performance are discussed separately (Li et al., 2014).

The data used for model evaluation include measurements of surface wind speed and direction (24 sites within Domain 4). These wind fields are obtained from two networks: the AZMET (ag.arizona.edu/azmet), and the Air Quality and Meteorological Information System (AQMIS) in the California EPA/Air Resources Board (www.arb.ca.gov/aqmis2/aqmis2.php). We use hourly observations of ozone concentrations from 26 stations in Arizona (downloaded from www.epa.gov/ttn/airs/airsaqs/) and 46 stations in Southern California (downloaded from www.arb.ca.gov/aqmis2/aqdselect.php?tab=hourly). In addition, the hourly NO_X observations, including four stations in Arizona and over 20 sites in southern California, and hourly CO observations, including four stations in Arizona and about 20 stations in southern California, can be obtained from the same websites as ozone data. Comparison of simulated and observed VOC

concentrations was precluded by the latter's irregular availability and their lack of hourly concentrations.

3. Results and discussion

Two episodes (May 14, 2012, and July 19, 2005) are selected as case studies. The criterion for selection required observed DMA8 [O_3] to exceed 80 ppbv for at least 10 of the reporting stations in the Phoenix metropolitan area. For both events, the synoptic weather in southern California and south-central Arizona was calm, clear, and sunny with light westerly winds within the lower troposphere for the time periods discussed in this section, based on NARR 3-hourly data. In addition, these two events represent the pre-monsoon and monsoon seasons, respectively, two typical climate circulations (Adams and Cowrie, 1997) during the ozone season.

The model (WRF-Chem) is initialized four days prior to each episode with the data of the first 24hours being discarded. In addition, analysis nudging is applied for the meteorological fields (U, V, T, GPH, and Q) above the PBL in the outer-most domain for the first 24 hours.

3.1 Model evaluation

Figure 2 shows the comparison of surface wind fields (circles in Figure 1b) between observations (bold-black) and WRF-Chem simulations (bold-red; i.e., running WRF-Chem with appropriate emissions and hereafter referred to as CTRL) for the selected events. The time periods (labeled in figure 2) cover 4 days, concluding with the episode day in the Phoenix metropolitan area. In comparison with observations, the model appropriately reproduced the diurnal variation with only a slight overestimate of wind speed during daytime. Note that each

observation represents a single point while the closest simulation grid cell to the observed latitude/longitude location (representing an area of 1.333 by 1.333-km) is used for comparison. Although there are some differences between simulated and observed means, the standard deviations for both modeled (thin-red) and observed (thin-black) measurements fall in the same range. Mean Bias (MB), Root Mean Squared Error (RMSE), and correlation coefficient (R) are also calculated and labeled in each panel. For the U-component of wind speed, MB is less than 1.0 m/s and RMSE is about 3.0 m/s (indicating wind heterogeneity within the simulation domain). U-component winds for the CTRL runs and the observations exhibit linear correlations with statistical significance ($P<0.01$). The MB for V-component wind is less than 0.5 m/s. Linear correlation indicates that V-component winds from the model and the observations are statistically significant ($P<0.01$) for the time periods of May 11-14, 2012 and July 16-19, 2005. The wind and temperature comparisons between WRF-Chem in Domain 1 and NARR data are also examined. Generally, the simulations are consistent with NARR data in patterns and magnitudes for the two cases. More specifically, there were continuously westerly winds between the southern California and central Arizona for both NARR and simulations at 850 hPa. Figure S1 is an example of the comparisons of wind and temperature at 850 hPa (bottom panel) and 700 hPa (top panel) for the average of July 16-19, 2005. These comparisons, which indicate sufficiently accurate meteorological simulations, ensure that regional pollutant transport can be adequately simulated, one of our focuses in this study.

Figure 3 shows the comparison of CO, NOx, and O_3 concentrations between the model (bold-red, i.e., CTRL run) and observations (bold-black) in Domain 4 for the same time periods. Note that only four sites of NOx and CO were measured (only one site online available) in greater

Phoenix while over 20 sites are found in southern California. On average, the model performed well for both CO and NOx concentrations for the July case. In contrast, for the May case, the model overestimated CO and NOx during nighttime but matched observations during daytime. The standard deviations (thin-red) from the model are much greater than those from observations (thin-black), indicating that modeled NOx and CO heterogeneity at sites is greater than that from observations. The model behavior in the May case indicates that the anthropogenic emissions could be over-estimated using the NEI05 data due to emission control strategies enacted in California in the seven intervening years (Pusede and Cogen, 2012). Figure S2 shows how the emissions changed between 2005 and 2012 for the South Coast Air Basin, California (http://www.arb.ca.gov/app/emsinv/fcemssumcat2013.php) and 2011 in Maricopa County, Arizona (http://maricopa.gov/aq/divisions/planning_analysis/emissions_inventory/Default.aspx) Relative to 2005, anthropogenic emissions of CO, NOx, and VOC are reduced about 40-50% in 2012 in the South Coast airshed, California. Therefore, the NEI 2005 overestimates [CO] and [NOx]. However, the changes in Maricopa County are not significantly except CO from Mobile.

The $[O_3]$ comparison between observations and simulations presented in Figure 3 indicates the model performed better in simulating $[O_3]$ than CO or NOx. Both the station average and station standard deviation from the model and observations matched each other on event and non-event days (details on site-by-site comparisons in Phoenix will be discussed in the next section). The simulated average $[O_3]$ and their spatial heterogeneities fall within the range of observations except on May 13, 2012, when modeled average $[O_3]$ and the spatial standard deviations fall out of the observation ranges.

Figure S3 shows [O_3] time series separately for southern California and greater Phoenix; corresponding statistics are shown in Table 1. In checking Figure 3, and Figures S2 and S3, although the NEI-2005 over-estimated CO and NOx emissions in 2012 in the south coast airshed, California, causing [NOx] and [CO] to be over-estimated as well, the ozone simulations nonetheless appear to be quite acceptable. One explanation could be that this airshed is categorized as a VOC-limited ozone environment. Under this condition, ozone concentrations are restrained by VOC concentrations. In other words, reducing NOx fails to reduce ozone concentrations (e.g.,Taha et al., 1998) and the same is also found in Phoenix area (Fast et al., 2000, Lee and Fernando, 2013), which can partly explain why the modeled [O_3] matched the observations, even though the modeled [NOx] and [CO] are highly overestimated in the May case.

Table 1 presents the statistics of comparisons of surface ozone concentrations between the model and observations in southern California (total 46 sites) and greater Phoenix area (total 24 sites), respectively. These statistics are widely used in evaluating model performance (Simon et al., 2012). Our statistics are comparable with those from previous studies in the two regions. For example, in southern California, the mean biases, RSME and correlation coefficients shown in Table 1 are comparable with those from Huang et al.(2013, their Table 3) and Chen et al. (2013, their Tables 2 and 3). Furthermore, the mean normalized bias and mean normalized gross error are comparable with those from Taha (2008, in his Table 2). In greater Phoenix, these statistics are generally comparable with those from Lee et al. (2007), and Li et al. (2014).

To examine the effects of model resolution on surface ozone concentrations, we conducted two additional model runs. These two additional runs were set up and configured exactly the same as the 1.33 km runs; but, with just running WRF-Chem with Domains 1, 2, and 3, which means the highest resolution of model output is 4 km. The model performance at 4 km resolution was also validated against ozone observations and summarized in Table 1. As shown in Table 1, the model performed much better for the correlation coefficients, normalized mean gross errors, mean normalized bias, and normalized mean error at 1.33 km than those at 4 km. For the mean bias and normalized mean bias, the model performed better in southern California at 1.33 km than those at 4km, with similar performance in greater Phoenix. Therefore, we conclude that WRF-Chem in its present configuration performed better at 1.33 km resolution than that at 4 km resolution, based on the two events and on the 2005 NEI. Our results are consistent with previous studies (e.g., Taha 2008; Tie et al., 2010). In the following analysis and discussion, we mainly focus on the model output at 1.33 km resolution.

The evaluation shown in Figs. 2-3, Figure S3, and the statistical analysis presented in Table 1 demonstrate that the WRF-Chem model, in its current configuration and set up, produces simulated ozone concentrations comparable to the observations.

3.2 Contribution of local and remote emissions to Phoenix [O_3]

Next, we investigate impacts of anthropogenic emissions in southern California (SoCal) and Arizona (AZ) on Phoenix [O_3]. To achieve this goal, we have conducted additional WRF-Chem simulations for the selected cases with the same model setup as presented and evaluated in Sections 2.1 and 3.1, and refer to these experiments as “CTRL”, but with (1) exclusion of SoCal

emissions (indicated as the dashed-red-line box in Figure 1b) and called “noCA”; (2) exclusion of AZ emissions (indicated as the dashed-black-line box in Figure 1b) and called “noAZ”; and (3) exclusion of all anthropogenic emissions in Domain 4, and called BIogenic emissions and Lateral Boundary inflow (BILB).

Figure 4 shows the hourly [O_3] comparison for observations (Obs), CTRL, noCA, noAZ, and BILB simulations at selected observation sites in the Phoenix area on May 11-14, 2012, (Figure 4a-4f) and July 16-19, 2005 (Figure 4g-4l). Figure 4 indicates that hourly [O_3] from the CTRL run match the observations very well in western downtown (ID0019, ID2001), central downtown (ID3003, ID9997), and east and north suburban areas (ID9508, ID9702). AZ emissions are the principal contribution to ozone production over Phoenix during daytime (compare the change in simulated [O_3] as demonstrated by the red contour [CTRL] and dashed-blue contour [noAZ]), with a maximum magnitude of up to 40-60 ppbv hourly (compare differences between CTRL and noAZ). The contribution of SoCal emissions to Phoenix [O_3] ranges between 10-40 ppbv during daytime (compare the change in simulated [O_3] as demonstrated by the red contour [CTRL] and green contour [noCA]). Based on the BILB run (gray contour), the contribution of biogenic emissions (including larger-scale lateral input) to Phoenix [O_3] varies between 25-35 ppbv, indicating a baseline target for emission reduction strategies. Following Huang et al (2013), the contribution of SoCal to [O_3] in the Phoenix area is the difference between the CTRL and noCA experiments. The relative contributions from SoCal, AZ, and BILB emissions to hourly [O_3] at observation sites for July 19, 2005 and May 14, 2012 are shown in Figures S4 and S5.

Figure 4, and Figures S4 and S5 indicate the relative contribution of SoCal and AZ emissions to [O_3] vary with time. Physical and chemical processes at each stage can explain this

335 variation. During nighttime, noCA [O_3] are less than that of the noAZ run. This is because there is
336 no ozone consumption (or titration) in the noAZ run while transported ozone can still make its
337 contribution. After sunrise, solar radiation heats the ground surface, increasing the planetary
338 boundary layer (PBL) height. Ozone accumulated within a residual layer from previous day(s) is
339 entrained into the PBL, increasing ground-level [O_3]. This process continues until the PBL height
340 reaches its peak. Simultaneously, ozone production starts with its precursor emissions in the
341 presence of sunlight, a rate that increases with increasing sunlight intensity and surpasses the
342 transport rate of [O_3] by mid to late afternoon. Furthermore, the figures indicate that the peak
343 time of [O_3] differs between the CTRL run and the noAZ run at some locations for some days.
344 These differences of [O_3] peak time indicate the importance of ozone transport. Figure 5 displays
345 the mean diurnal variation of [O_3] for the different emission scenarios for the two cases. The data
346 are averaged over all urban grid cells (i.e., not solely over the station sites presented in Figure 4)
347 in Phoenix for May 11-14, 2012, and July 16-19, 2005, respectively. The relative contribution of
348 emissions to Phoenix [O_3] are clear and the diurnal features are similar to those shown in Figure
349 4, and Figures S4 and S5, emphasizing the crucial roles of both local and remote emissions.
350 The daily maximum 8-hr average (DMA8) [O_3] from CTRL and the relative contributions to
351 DMA8 [O_3] from different emission scenarios (BILB, SoCal, and AZ) are assessed at observation
352 sites and for all urban grid cells within Phoenix (Figure 6).The model reproduces observations
353 very well with a slight underestimation on July 19, 2005, but with an overestimation on May 13,
354 2012. The contribution of SoCal to DMA8 [O_3] in the Phoenix area ranges between 20 – 30 ppbv
355 for the May case and 5 - 20 ppbv for the July case. Relative to the CTRL run, the percentage
356 contributions of 26% - 36% for the May case and 7% - 38% for the July event emphasize the

357 significant effect of southern California emissions on Phoenix metropolitan area air quality. For
358 the two episode days, the contributions are 28 ppb (36%) for May 14, 2012, and 11 ppb (16%)
359 for July 19, 2012. The relative contributions of AZ local emissions to greater Phoenix observation
360 sites are also shown in Figure 6. Overall, the relative contributions of AZ local emissions to
361 Phoenix [O_3] are more than that of SoCal emissions.

362 The means of DMA8 [O_3] throughout the Phoenix urban area (about 1100 grid cells)
363 arising from the different emission scenarios are shown in Figure 6b and d, and indicate similar
364 values to those at observation sites (Figure 6a, c). The contribution of SoCal emission to DMA8
365 [O_3] for the Phoenix metropolitan area ranges between 20 – 32 ppbv for the May 11-14, 2012,
366 case, and from 6 – 22 ppbv for the July 16-19, 2005, case. The percentages, relative to CTRL, are
367 from 27% to 37% for May 11-14, and from 9% to 40% for July 16-19. Considering only the two
368 days with the maximum ozone concentrations, the contributions are 29 ppb (37%) and 11 ppb
369 (16%) for May 14, and July 19, respectively.

370 Note that in Figure 6, the differences of CTRL minus BILB is not equal the sum of the
371 differences of CTRL minus noCA plus that of CTRL-noAZ. The reason could be the nonlinear
372 processes among emissions, physical, and/or chemical mechanisms (Kwok et al. 2015) and the
373 uncertainties of the entire system: both the emissions and the models themselves.

374

375 Figure 6 demonstrates the following results: (1) the impact of AZ emissions on DMA8 [O_3]
376 in the Phoenix area is greater than that of the SoCal's; (2) even so, SoCal emissions considerably
377 increase DMA8 [O_3] in the Phoenix area by up to 30 ppbv, though this is day and case dependent;
378 (3) the DMA8 [O_3] from the BILB experiment are in excess of 30 ppbv, including the contributions

379 of biogenic emissions and lateral boundary transport. Based on the diurnal variations shown in
380 Figures 4 and 5, and Figures S4 and S5, [O_3] due to biogenic emissions and lateral boundary inflow
381 could be 10-17 ppbv. In other words, the contribution of BILB to Phoenix DMA8 [O_3] cannot be
382 ignored despite the region's aridity and lack of dense forests. Note that all of these results are
383 based on the US EPA 2005 national emissions inventories.

384 Figure 7 depicts the spatial distributions of DMA8 [O_3] for different emission scenarios on
385 July 19, 2005. The CTRL run indicates that higher [O_3] occur in the northeastern urban perimeter,
386 which is consistent with previous studies (e.g. Lee and Fernando 2013). The effects of SoCal
387 emissions and AZ local emissions on DMA8 [O_3] are location-dependent. The case of May 14,
388 2012, is also examined (see Figure S6) and a similar distribution as in Figure 7 is found, but it
389 differs in magnitude.

390 In summary, our results demonstrate that removing SoCal emissions would facilitate
391 attainment of [O_3] in Phoenix on some days, but not on others. In other words, SoCal emissions
392 are an important, if uneven, contributor to the DMA8 [O_3] exceedances for Phoenix. In addition,
393 the effects of SoCal emissions on Phoenix DMA8 [O_3] are location-dependent (see Figure 7 and
394 Figure S6). From a pollution control point of view, our results indicate that reducing the emissions
395 emitted in Phoenix is the key to attain federal standards. With typical synoptic wind fields,
396 emissions from southern California affect ground-level [O_3] in the Phoenix metropolitan area
397 significantly. Therefore, the results indicate that Phoenix would benefit from regional, in addition
398 to local, emission controls to reach NAAQS attainment status.

399

400 **3.3 Southern California to Arizona [O_3] transport**

401 Through analysis of [O_3] variations with the various emission scenarios, 10-30% of [O_3] in
402 the Phoenix area can be attributed to SoCal emissions for the cases presented here. In this section
403 we will examine pathways characterizing how pollutants in the coastal air basins of southern
404 California are transported into Arizona and affect air quality in the Phoenix area based on 1.33
405 km resolution model output. The corresponding analyses of the results from the 4 km resolution
406 output can be found in the supplement materials.
407 Figure 8a shows a Hovmoller diagram of [O_3] differences (CTRL minus noCA) and the wind
408 vector field (from CTRL run) for the May case at the model's 13th vertical level (about 1100 m
409 above ground-level, or a.g.l.) of WRF-Chem along the cross-section B'B (indicated in Figure 1b).
410 The Hovmoller diagram is a suitable technique to identify transport and propagating phenomena
411 in a given field (i.e. Hovmoller, 1949). In Fig. 8a, the y-axis is the model integration time (hours)
412 and the x-axis is the location (longitude) along the B'B transect. The approximate locations of
413 Phoenix (PHX), desert, mountains (Mnts) and coast are also labeled in this figure. Since both CTRL
414 and noCA experiments include the same emissions except over California, the difference in ozone
415 between these experiments offsets the chemical ozone production east of California and west of
416 Phoenix. Thus, the residual ozone perturbation field in these regions is dominated by transport.
417 The pattern of this field exhibits tilted ozone bands with phase lines that have consistent positive
418 slopes (Fig. 8a), indicating that a perturbation of ozone in California will eventually reach Arizona.
419 This demonstrates that the residual ozone field shown in Fig. 8a is caused by transport from
420 California to Arizona. The Hovmoller diagram of [O_3] differences for the July case also exhibits
421 patterns of residual ozone with positive slopes indicating transport (Fig. 8b). These slopes are,
422 however, less pronounced than the May case.

423 The data within each model vertical layer are examined. It is found that peak transport
424 occurs in different model layers depending on the event. For the July event, there is ozone
425 transport from the 5th model layer (about 150 m a. g. l.) to the 13th model layer(1100 m a. g. l.).
426 For the May event, ozone transport occurs from the 5th to 17th (2000 m a. g. l.) model layers. The
427 Hovmoller diagrams for NOx and VOCs indicate that most air masses of NOx and VOCs are
428 horizontally confined near emission source areas and are vertically restricted to below about
429 1500 m a.g.l. (figure not shown), compared to the magnitude presented in Figure 8.

430 We next examine how pollutants from southern California are transported into south-
431 central Arizona and discuss the physical-chemical mechanisms responsible. Analysis of
432 anthropogenic emission distributions indicates that emissions mainly originate from coastal
433 areas in southern California (also see their Figure 1 in Chen et al. 2013 for emission distribution).
434 Therefore, we first explain how the pollutants cross the coastal mountains and reach the inland
435 desert regions in southern California.

436 As discussed in Section 1, wind fields are paramount in pollutant transport (Lee et al.,
437 2007). Figure 9 displays the daytime averaged (20Z to 02Z) wind vector field at 40 m a. g. l. in the
438 southern California coastal area of July 16-19, 2005 (for 4 km resolution plots, see Figure S7). The
439 wind patterns exhibit a combination of on-shore ocean breezes and mountain-induced upslope
440 winds, similar to features reported by Lu and Turco (1996) and Lu et al. (1997). The wind field
441 distribution shown in Figure 9 propels pollutants emitted in coastal areas towards the coastal
442 mountains. The polluted air masses can be lofted up to 3-4 km a.g.l. over the mountains through
443 the Mountain Chimney Effect (MCE, Lu and Turco, 1996). The pollutants above mountain-top
444 height might either be transported into the free atmosphere over the coast (Lu and Turco, 1996)

445 and/or be transported towards the inland desert and affect the air quality in the desert of
446 southern California (Huang et al. 2013; VanCuren 2014) and of nearby mountain states (Langford
447 et al. 2010; Huang et al. 2013).

448 The entire transport path, from the southern California coast to south-central Arizona,
449 and the associated ozone vertical distributions along cross-sections A'A, B'B, D'D and E'E, is
450 described here in this subsection. First, vertical distributions of [O_3] along cross-sections A'A and
451 B'B are checked from 21Z to 24Z each day and Figure 10 is an example of vertical distributions of
452 [O_3] along cross-section A'A and B'B at 22Z on July 17, 2005 (for 4km resolution plots, see Figure
453 S8). Results presented in Figure 10 are similar to those reported by Lu and Turco (1996, in their
454 Figures 4 and 6) from modeling and Langford et al (2010; in their Figure 3) from observations,
455 indicating that WRF-Chem adequately simulates the Mountain Chimney Effect (MCE). Note the
456 distribution of potential temperature contours in Figure 10, illustrating that ozone-laden air
457 masses above mountain peak height may be directly transported into the desert PBL under
458 appropriate flow at these levels. This pattern differs from that of transport back to the free
459 atmosphere over coastal basins (note the tongue of high [O_3] to the west of the peak in Figure
460 10a). This is because of the particularly high PBL height (in excess of 3-4 km a. g. l.) in the desert
461 during daytime due to strong solar radiation. At nighttime, ozone air masses subsequently
462 subside into the residual layers and/or stable PBL in the desert, and are continuously advected
463 by westerly winds (part of the near-surface ozone will be consumed by titration from NOx and
464 by deposition during nighttime). Importantly, Figure 9 indicates the presence of strong winds
465 from the coast flowing through the mountain passes. For example, there are southerly winds
466 flowing along the Cajon Pass (see location in Figure 1b) and strong westerly winds flowing along

467 the San Gorgonio Pass (see location Figure 1b), which are realistic and consistent with the
468 immense fields of wind turbines there. With the wind pattern shown in Figure 9, ozone in low air
469 layers can be directly transported into the southern Mojave Desert Air Basin (SMDAB, See Figure
470 1b) from the greater Los Angeles Air Basin (GLAAB) through the Cajon Pass. Ozone can also be
471 transported eastward to the Salton Sea Air Basin (SSAB) from the GLAAB through the San
472 Gorgonio Pass and from the San Diego Air Basin (SDAB) through other passes (see Figure 9 for
473 the locations and wind vectors).

474 To demonstrate the model performance in simulating [O_3] in the passes, Figure 11
475 presents the hourly comparison of [O_3] between observations and simulations (CTRL) at Crestline,
476 near the Cajon Pass, and Banning Airport, near the San Gorgonio Pass. Figure 11 shows that the
477 simulations and the observations are comparable from July 17 to July 19, 2005. In Figure 11,
478 model simulations with 12-km resolution are also plotted to characterize resolution-dependency.
479 It is clear that with higher-resolution, simulated results are improved above those of coarser
480 resolution, a feature likely due to more accurate ozone transport through the passes.

481 Figure 12 shows the horizontal distribution of the integrated fluxes of ozone differences
482 ($\int([O_3]_{CTRL} - [O_3]_{noCA})\vec{V}_{CTRL}\,dz$) from the surface to 1400 m a.g.l. averaged from (a) 18Z to 02Z
483 and (b) 03Z to 17Z, July 16-20, 2005 (data from the other case May 11-15, 2012 are similar and
484 for 4 km resolution plot, see Figure S9). Figure 12 emphasizes two key aspects of this transport:

485 (1) There were stronger fluxes in the mountain passes, especially in the San Gorgonio
486 Pass, than any other location, indicating the important contributions of mountain passes
487 to ozone transport. Most recently, VanCuren (2014), based on analysis of ozone

observations, also suggests the importance of ozone transported into the MDAB through the passes and has confirmed our model results.

(2) Ozone fluxes are present, originating from the coasts and mountains in southern California, extending southeastward along the SSAB and the SMDAB (Figure 12b), crossing the California-Arizona border near the southern Colorado River, then moving northeastward (Figure 12b) along the Lower Gila river basin, and finally reaching the Phoenix area.

The vertical distribution of pollutants is also evaluated along cross-section D'D in the Salton Sea Valley and cross-section E'E in the Gila River Valley (locations are labeled in Figure 1b). Presenting vertical distributions of VOC, NOx and O_3 along D'D on July 18 from CTRL, Figure 13 depicts the transport of the pollutants from late afternoon to midnight, as indicated by the location of high concentration fronts(for the corresponding 4 km resolution plots, see Figure S10). The NOx masses are vertically confined to below 1-km above sea level (asl) with concentrations of 5-15 ppbv. VOC plumes are confined below 2-km asl with concentrations of 10-20 ppbv. We also evaluated the vertical distribution of VOC from the BILB emissions experiment: the vertical distribution is similar to the VOC shown in Figure 13, but the concentrations are about 10 ppbv (figure not shown). In other words, there are about 10 ppbv of VOC that are transported from coastal anthropogenic emissions to this region. Similar to NOx concentrations, the highest concentrations of VOC are near the ground surface.

Ozone vertical distributions reach up to 2-3 km a.s.l. with concentrations as high as 90 ppbv. The high [O_3] is centered 1-2 km a.s.l. during nighttime while [O_3] is low near ground-level

509 due to the chemical titration by NOx and dry deposition (Figure 13). In other words, among the
510 three pollutants, ozone is most “long-lived” and NOx has the shortest span, which is consistent
511 with their atmospheric chemistry and previous results (e. g., Lee and Fernando, 2013).

512 The diurnal variation of a pollutant is, in part, a consequence of diurnal variation of flow
513 (the other principal influence is the diurnal variation of the emissions themselves). During
514 daytime, southeasterly winds (valley winds) at lower layers in the northern Salton Sea basin
515 hinder the pollutants from being transported southeastward along the Salton Sea Basin (See
516 Figure 12a and Figure 9). Therefore, a portion of the pollutants, transported from the GLAAB
517 through the San Gorgonio Pass, accumulate over the northern Salton Sea basin (as shown at 01Z
518 in Figure 13), while a different portion of the pollutants crossed the Little San Bernardino
519 Mountains and reached the SMDAB due to upslope flow (see Figure 12a and Figure 9). During
520 nighttime, basin-scale mountain downslope winds transport the pollutants southeastward along
521 the SSAB basin (Figure 12b and Figure 13).

522 Figure 14 is similar to Figure 13 but presents results for the cross-section E’E in the Gila
523 River basin in Arizona (location shown in Figure 1b) on July 18 (corresponding 4 km resolution
524 plots, see Figure S11). During this time period, although concentrations of pollutants continued
525 to decrease along this transport pathway, the ozone transport phenomenon was still very clear
526 along the Gila River basin due to the prevailing nighttime southwesterly winds (see Figure 12).
527 These southwesterly winds can result from either the low-level jet from the northern Gulf of
528 California during monsoon season (mid-July to mid-September), Adams and Comrie, 1997) or by
529 the inertia from a remnant of daytime westerly winds during pre-monsoon season (from May
530 to mid-July , Lee and Fernando, 2013). At about 18Z, the ozone in the residual layer mixes with

PBL ozone generated by local photochemical reactions, and finally affects the ground-level concentrations in Phoenix and its surrounding rural areas.

The results presented in this section are mainly based on model simulations. In past decades, there were a few field experiments conducted to measure the vertical distributions of meteorological fields and trace gasses in southern California (e.g., the southern California Air Quality Study in 1987 [Lawson, 1990]; the southern California Ozone Study in 1997[Groes and Fujita, 2003] and CALNEX-2010[www.esrl.noaa.gov/csd/calnex/]) as well as in the Phoenix area (e.g., Phoenix Air Flow Experiment II in 1998 [Fast et al. 2000; Nunnermacker et al., 2004]). Some of the events during the experiments have been used to address ozone transport (e.g., Huang et al. 2013; Langford et al., 2010) from the southern California coast. No aloft measurements could be found for May 2010 that would be of help in the present model performance evaluation. In addition, satellite-retrieved data may be used to demonstrate the vertical distributions and even distant transport (e.g., Huang et al., 2013), although these data are hampered by limitations such as coarse-resolution, accuracy, etc. (e.g., Bowman, 2013). To quantitatively examine the transport and vertical distribution from southern California coasts to Phoenix, field observations, especially measurements aloft, along the inland California desert region and within western Arizona are needed.

4. Conclusion

As with other cities, Phoenix's ozone concentrations on exceedance days can be attributed to both local precursor emissions and to the transport of ozone and its precursors from remote regions. In this study, WRF-Chem at high-resolution (~1.333-km grid spacing) is

553 employed to investigate surface ozone distributions in southern California and south-central
554 Arizona for two selected Phoenix episodes. Model simulations have been compared with surface
555 observations of hourly ozone, CO, NO_X and wind fields in southern California and Arizona. The
556 results indicate that the WRF-Chem configuration in this study can adequately simulate the
557 spatial distribution, the magnitude, and the variability of the observations. The modeled ozone
558 concentrations ($[O_3]$) are comparable with previous studies in the focus region.

559 Three sensitivity studies have been conducted to separate the contributions of southern
560 California anthropogenic emissions (SoCal), of the Arizona local anthropogenic emissions (AZ),
561 and of biogenic emissions and lateral boundary input to Phoenix $[O_3]$ on the exceedance days:
562 (1) running WRF-Chem as CTRL but excluding SoCal emissions (noCA), (2) running WRF-Chem as
563 the Control simulation but excluding AZ emissions (noAZ) and (3) running WRF-Chem as the
564 Control simulation but excluding all anthropogenic emissions in domain 4 areas, leaving the
565 BIogenic emissions and Lateral Boundary input (BILB). Our simulations indicate that AZ emissions
566 play the key role in formation of the elevated $[O_3]$ in Phoenix for the selected cases (see Figures
567 4, 5, and 6). Based on the US EPA 2005 emissions inventories, SoCal emissions contribute to
568 DMA8 $[O_3]$ in the Phoenix area, and this impact varies between 5-30 ppbv at various observation
569 sites and from 6-32 ppbv throughout the urban setting. In addition, our model simulations
570 indicate the effects of SoCal emissions on DMA8 $[O_3]$ in Phoenix are location and event
571 dependent, but not negligible. The effects of BILB contributions to Phoenix DMA8 $[O_3]$ are also
572 significant in spite of the region's aridity. Our future research will distinguish biogenic and lateral
573 boundary inflow contribution to this area through model simulations and observations. The
574 model results are based on the 2005 U.S. National Emissions Inventories (NEI 2005). With more

575 stringent emission control strategies in California, the effects of the pollutants transported from
576 California could be reduced.

577 The time series of [O_3] of the relative contributions to Phoenix [O_3] from SoCal and AZ
578 emissions exhibit a diurnal variation. During nighttime hours, the transported ozone increases
579 [O_3] while local NOx emissions consume it. The reverse occurs during afternoon hours when
580 locally generated emissions predominate.

581 WRF-chem's high resolution resolves all pertinent topographical features, especially the
582 critical low-elevation mountain passes, capturing the pollutant transport through them.
583 Therefore, the pollutant's (mainly ozone) transport pathway in the lower troposphere is
584 identified: The pollutants (mainly ozone) are first transported to the southern Mojave Desert Air
585 Basin (SMDAB) and the Salton Sea Air Basin (SSAB) through both the Mountain Chimney Effect
586 (MCE) and Mountain Pass Channel Effect (PCE) during daytime, affecting DMA8 [O_3] in these two
587 air basins. The following physical transport paths (based on the two events) are: the pollutants
588 are first transported southeastward along the two air basins (the SSAB and the SMDAB) in CA
589 during nighttime, then northeastward along the Gila River basin in AZ during nighttime, and
590 finally reach the Phoenix area and mix with the local air mass by turbulent mixing during daytime.
591 The entire transport path is determined by a combination of local and synoptic circulations.

592 Since the PBL height can extend in excess of 3-4 km a.g.l. in desert air basins, pollutants
593 may be directly transported into the daytime desert PBL from coasts by both PCE and MCE.
594 Therefore, regional transport in the desert is accomplished in the PBL (daytime), and residual
595 layer and stable PBL (nighttime).

596 **Acknowledgements**: This work has been funded by National Science Foundation grants DMS-
597 1419593 and EAR-1204774, and USDA NIFA grant 2015-67003-23508. We thank the Julie Ann

598 Wrigley Global Institute of Sustainability at Arizona State University for valuable support. The
599 authors appreciate the comments and suggestions from Dr. Steven Peckham (NOAA). Dr. Chun
600 Zhao (PNNL) and Dr. Xiaohong Liu (University of Wyoming) have also shared their successful
601 experiences with the first author. We are grateful to Dr. Kirk Baker (EPA) and the other Reviewer
602 for the comments and suggestions.

603 **References**

604 Ackermann, I., Hass, H., Memmesheimer, M., Ebel, A., Binkowski, F., and Shankar, U.: Modal
605 aerosol dynamics model for Europe: Development and first applications, Atoms.
606 Environ., 32, 2981-2999,1998.

607 Adams, D., and Cowrie, A.: The North American monsoon, BAMS, 78(10), 2198-2213, 1997.

608 Anderson, H.: Air pollution and mortality: A history, Atmos. Environ., 43,143-152,
609 doi:10.1016/j.atmosenv.2008.09.026,2009.

610 Ashmore, M. : Assessing the future global impacts of ozone on vegetation, Plant Cell Environ.,
611 29, 949-964, doi:10.1111/j.1365-3040.2005.01341.x.,2005.

612 Avnery, S., Mauzeral, D., Liu, J., and Horwiz, W. : Global crop yield reductions due to surface
613 ozone exposure: 1: Year of 2000 crop production losses and economic damage, Atmos.
614 Eviron., 45, 2284-2296,2011.

615 Bowman, K.: Toward the next generation of air quality monitoring: Ozone, Atmos. Environ., 80,
616 571-583, 2013.

617 Chameides, W., Li, X., Tang, X., Zhou, X, Luo, C., Kiang, C., St John, J., Saylor, R., Liu, S., Lam, K,
618 Wang, T., and Giorgi, F. : Is ozone pollution affecting crop yields in China? *G*epphys. Res.
619 Lett., 26, 867-870, doi:10.1029/1999gl900068,1999.

620 Chen D. , Li Q., Stutz J. , Mao Y., Zhang L., Pikelnaya O., and Tsai J.: WRF-Chem simulation of
621 NOx and O3 in the LA basin during CalNex 2010, Atmos. Environ., 81**,** 421-432.,2013.

622 Chen F., and Dudhia J.: Coupling an Advanced Land Surface Hydrology Model with the Penn State
623 NCAR MM5 Modeling System. Part 1: Model Implementation and Sensitivity, Mon.
624 Weather Rev*.,* 129**,** 569–585,2001.

625 Chen F., Kusaka H., Bornstein R., Ching J., Grimmond C., Grossman-Clarke S., Loridan T., Manning
626 K., Martilli A., Miao S., Sailor D., Salamanca F., Taha H., Tewari M., Wang X., Wyszogrodzki
627 A., and Zhang C.: The integrated WRF/urban modeling system: development, evaluation,
628 and applications to urban environmental problems, International J. Climatol., 31(2), DOI:
629 10.1002/joc.2158., 2011.
630 Cores B., and Fujita E.: Overview of the 1997 southern California ozone study(SCOS97-NARSTO),
631 Atmos. Environ.,37,3-26.doi:10.1016/S1352-2310(03)00379-0., 2003.
632 Ek M., Mitchell B., Lin K., Rogers Y., Grunmann E., Koren P., Gayno V. , and Tarpley J.:
633 Implementation of Noah land surface model advances in the National Centers for
634 Environmental Prediction operational mesoscale Eta Model, J. Geophys. Res., 108**,** 8851,
635 doi:10.1029/2002JD003296, 2003.
636 Emmons L., Walters S., Hess P., Lamarque J., Pfister G., FillmoreD., Granier C., Guenther A., Kinnison D.,
637 Laepple T., Orlando J., Tie X., Tyndall G., Wiedinmyer C., Baughcum S. L., and Kloster S.: 2010:
638 Description and evaluation of the model for ozone and related chemical traces, version 4
639 (MOZART-4), Geosci. Model Dev., 3**,** 43-67,2010.
640 EPA, 2014: National Ambient Air Quality Standards for Ozone, available online
641 (http://www.epa.gov/glo/pdfs/20141125proposal.pdf)
642 Fast J., Doran J., and Shaw W.: The evolution of the boundary layer and its effect on air chemistry
643 in the Phoenix area, J. Geophys. Res., 105(D18), 22833-22848,2000.
644 Fast J., Zaveri D., Bian X., Chapman E., and Easter R, 2002: Effect of regional-scale transport on
645 oxidants in the vicinity of Philadelphia during the 1999 NE-OPS field campaign, J. Geophys.
646 Res., 107(D16) 4307, doi:10.1029/2001JD000980, 2002.

Friedl M., McIver D., Hodges F., Zhang X., Muchnoey D. , Strahler A., Woodcock C., Gopal S., Schneider A., Cooper A., Baccini A., Gao F., and Schaaf C.: Global land cover mapping from MODIS: algorithms and early results, Remote Sens. Environ., 83, 287–302,2002.

Ginoux P., Chin M., Tegen I., Prospero J., Holben B., Dubovik O., and Lin S-J.: Sources and global distributions of dust aerosols simulated with the GOCART model, J. Geophys. Res., 106**,** 20255–20273,2001.

Grell G., and Devenyi D.: A generalized approach to parameterizing convection combining ensemble and data assimilation techniques, Geophys. Res. Lett., 29**,** 4pp. doi:10.1029/2002GL015311, 2002.

Grell G., Peckham S., Schmitz R. , McKeen S., Frost G. , Skamarock W., and Eder B.: Fully coupled "online" chemistry within the WRF model, Atmos. Environ. 39**,** 6957–6975, doi:10.1016/j.atmosenv.2005.04.027, 2005.

Gross A., and Stockwell W.: Comparison of the EMEP, RADM2 and RACM mechanisms, *J. Atmos. Chem.,* 44(2), 151-170, 2003.

Guenther A., Karl T. , Harley P. , Wiedinmyer C. , Palmer P., and Geron C., 2006: Estimates of global terrestrial isoprene emissions using MEGAN (Model of Emissions of Gases and Aerosols from Nature), Atmos. Chem. Phys., 6**,** 3181–3210, doi:10.5194/acp-6-3181-2006, 2006.

He, H., Sehr, L., Hains, J., Krask, D., Dodridge, B., Vinnikov, K., Canty, T., Hosley, K., Salawitch, R., Worden,H., and Dickerson, R.: Trends in emissions and concentrations of air pollutants in the lower tropospheric in the Baltimore/Washington airshed from 1997-2011, Atoms. Chem. Phys., 13, 7859-7874, 2013.

669 Huang, M., Bowman, K., Carmichael, G., Pierce, B., Worden, H., Lou, M., Cooper, O., Pollack, I. Ryerson,
670 T., and Brown, S.: Impact of Southern California anthropogenic emissions on ozone
671 pollution in the mountain states: Model analysis and observational evidence from space,
672 J. Geophys. Res-Atmos., 118, 12784-12803, 2013.
673 Hovmoller, E, 1949: The trough-and-Ridge diagram, Tellus, 1(2), 62-66.
674 IPCC: Climate change, 2007: The physical science basis, contribution of Working Group I to the
675 Fourth Assessment Report (AR4) of the Intergovemental Panel on Climate Change,
676 996pp.
677 Kemball-Cook S., Parrish D., Ryerson T., Nopmongool U., Johnson J., Tai E., and Yarwood G.:
678 Contributions of regional transport and local sources to ozone exceedances in Houston
679 and Dallas: Comparison of results from a photochemical grid model to aircraft and
680 surface measurement, J. Geophys. Res*.,* 114**,** D00F02 doi:10.1029/2008JD010248, 2009.
681 Klich C., and FueIberg H.: The role of horizontal model resolution in assessing the transport of
682 CO in a middle latitude cycle using WRF-Chem, Atmos. Chem. Phys*.,* 14, 609-627, 2014.
683 Kwok R., Baker K., Napelenok S., and Tnonnesen G.: Photochemical grid model implementation
684 and application of VOC, NOx, and O_3 source apportionment, Geosci. Model Dev*,* 8: 99-
685 114. doi:10.5194/gmd-8-99-2015, 2015.
686 Langford A., Senff C., Alvarez R., Banta R., and Hardesty R.: Long-range transport of ozone from
687 the Los Angeles Basin: A case study, *Geophys. Res. Lett*, 37,
688 L06807,doi:10.1029/2010GL042507, 2010.
689 Lawson D., 1990: The southern California air quality study, J. Air Waste Manage. Assoc., 40,156-
690 165, 1990.

691 Lee S., Fernando H., Princevac M., Zajic D., Sinesf M., Mcculley J. and Anderson J. : Transport
692 and diffusion of ozone in the nocturnal and morning planetary boundary layer of the
693 Phoenix Valley, Environ. Fluid Mech., 3 331-362, 2003.
694 Lee S., and Fernando H.: Dispersion of an urban photochemical plume in Phoenix metropolitan
695 area, Atmos. Environ., 80**,** 152-160, 2013.
696 Lee S., Fernando H., and Grossman-Clarke S.: MM5-SMOKE-CMAQ as a modeling tool for 8-h
697 ozone regulatory enforcement: application to the state of Arizona, Environ. Model.
698 Assess.*,* 12**,** 63-74, 2007.
699 Levy II H., Mahlman J., Moxim W., and Liu S.: Tropospheric Ozone: The role of transport. J.
700 Geophys. Res., 90(D2), 3753-3772, 1985.
701 Li J., Georgescu, M., Hyde P., Mahalov A., and Moustaoui M.: Achieving accurate simulations of
702 urban impacts on ozone at high resolution. *Environ. Res. Lett*. 9(2014),114019, 2014.
703 Lin Y., Farley R., and Orville H. : Bulk parameterization of the snow field in a cloud model, *J.*
704 *Climate Appl. Meteor.* 22, 1065–1092, 1983.
705 Lin, M., Fiore, A., Horowitz, L., Cooper, O., Naik, V.,Holloway, J., Johnson, B., Middlebrook,
706 A., Oltmans, S., Pollack, I., Ryerson, T., Warner, J., Wiedinmyer, C., Wilson, J., and
707 Wyman, B.: Transport of Asian ozone pollution into surface air over the western United
708 States in Spring, J. Geophys. Res., 117, D00V07, doi:10.29/2011JD016961, 2012.
709 Lu R., and Turco, R.: Air pollution transport in a coastal environment: Part II: Three-
710 dimensional simulations of sea-breeze and mountain effect, Atmos. Environ., 29B, 1499-
711 1518, 1995.

712 Lu R., and Turco R.: Ozone distributions over the Los Angeles Basin: Three-dimensional
713 simulations with the SMOG model, Atmos. Environ., 30(24), 4155-4176, 1996.
714 Lu R., Turco R., and Jacobson M.: An integrated air pollution modeling system for urban and
715 regional scales: 2: Simulations for SCAQS 1987, J. Geophys. Res., 102(D5), 6081-6098,
716 1997.
717 MacDonald C., Miller, D., and Raffuse, D.: Regional and local contributions to peak local ozone
718 concentrations in six western cities. *Final Report for Western States Air Resources*
719 *Council (WESATR), STI-906004-2970-FR*, Sonoma Technology, Inc.
720 (www.sonomatech.com), 2006.
721 Mauzerall D., and Wang, X.: Protecting agricultural crops from the effects of tropospheric ozone
722 exposure: Reconciling science and standard setting in the United States, Europe, and Asia,
723 Ann. Rev. Energy Environ., 26, 237-268, 2001.
724 Mesinger F., DiMego, G., Kalney, E., Mitchell, K., Shafran, P., Ebisuzaki, W., Jovic, D., Woollen J.,
725 Rogers, E., Berbery, E., Ek, M., Fan, Y., Grumbine, R., Higgins, W., Li, H., Lin, Y., Manikin,
726 G., Parrish, D., and Shi, W.: North American regional reanalysis, *Bull. Amer. Meteor. Soc.,*
727 87**,** 343-360, 2006.
728 Mlawer E., Taubman S., Brown P., Iacono M., and Clough S.: Radiative transfer for
729 inhomogeneous atmospheres: RRTM, a validated correlated–k model for the longwave,
730 J. Geophy. Res.– Atmos., 102**,** 16663–16682, 1997.
731 Moore, T.: Ozone 301, Maricopa County Air Quality Department, September 4, 2014 (available:
732 http://www.wrapair2.org/WestJumpAQMS), 2014.

733 Nunnermacker L., Weinstein-Lloyd J., Kleinman L., Daum P., Lee Y., Springston S., Klotz P.,
734 Newman L., Neuroth G., and Hyde P.: Ground-based and aircraft measurements of trace
735 gases in Phoenix, Arizona (1998), Atmos. Environ., 38, 4941-4956, 2004.Peckam, S., Grell,
736 G., McKeen, S., Ahmadov, R., Barth, M., Pfuster, G., Wiedinmyer, C., Fast J Gustat]fason, W.,
737 Ghan, S., Zaveri, R., Easter, R., Barnard, J., Chapman, E., Hewson, M., Schmitz, R., Salzmann,
738 M., Beck, V., Freitas, S., Previsao de, C., and Estudos, T.:WRF/CHEM Version 3.5 User's Guide,
739 available at: ruc.noaa.gov/wrf/WG11/Users guide.pdf (last access: 12 February 2013), 2013.
740 Pusede A., and Cogen R.: On the observed response of ozone to NOx and VOCs reductions in San
741 Jaquan Valley California 1995-present, Atmos. Chem. Phys., 12, 8323-8339, 2012.
742 Schell B., Ackermann I., Hass H., Binkowski F., and Ebel, A.: Modeling the formation of secondary
743 organic aerosol with a comprehensive air quality modeling system, *J. Geophys. Res*., 106,
744 28275-28293, 2001.
745 Simon H., Baker K., and Phillips S.: Compilation and interpretation of photochemical model
746 performance statistics published between 2006 and 2012, Atmos. Environ., 61, 124-139,
747 2012.
748 Skamarock W., Klemp J., Dudhia J., Gill D., Barker D., Wang W. and Powers J.: A description the
749 Advanced Research WRF version 3, www.mmm.ucar.edu/wrf/users/docs/arw_v3.pdf,
750 2008.
751 Smith, K., Jerrett, M., Anderson, R., Burnett, R., Stone, V., Derwent, R., Atkinson, R., Cohen, A.,
752 Shonko, S., Krewski, D., Pope, III, A., Thun, M., and Thurston, G.: Public benefits of
753 strategies to reduce greenhouse-gas emissions: Health implications of short-lived
754 greenhouse pollutants, *Lancet*, 374(9707), doi:10.1016/S0140-6737(09)61716-5, 2009.

755 Stock Z., Russo M., and Pyle J.: Representing ozone extremes in European megacities: the
756 importance of resolution in a global chemistry climate model, Atmos. Chem. Phys., 14,
757 3899-3912, 2014.
758 Stockwell W, Middleton P. , Chang J., and Tang X.: The Second Generation Regional Acid
759 Deposition Model Chemical Mechanism for Regional Air Quality Modeling, J. Geophys.
760 Res., 95**,** 16343–16367, 1990.
761 Taha H.: Urban surface modification as a potential ozone air-quality improvement strategy in
762 California: A mesoscale modeling study, Boundary-layer Meteorol., 127, 219-239, 2008.
763 Taha H., Konopacki S, and Akbari H.: Impacts of lowered urban air temperature on precursor
764 emission and ozone air quality. J. Air Waste Manage. Assoc., 48, 860-865, 1998.
765 Tie, X., G. Brasseur, G., and Ying, Z., 2010: Impact of model resolution on chemical ozone
766 formation in Mexico City: application of the WRF-Chem model, Atmos. Chem. Phys., 10,
767 8983-8995, 2010**.**
768 Zhao C., Liu X., and Leung R. 2012: Impact of the desert dust on the summer monsoon system
769 over the southwestern North America, Atmos. Chem. Phys., 12, 3717-3731, 2012.
770 Zhao C., Liu, X., Leung R, Johnson B., McFarlane S., Gustafson Jr W., Fast J., and Easter R.,
771 2010: The spatial distribution of mineral dust and its shortwave radiative forcing over
772 North Africa: modeling sensitivities to dust emissions and aerosol size treatments,
773 Atmos. Chem. Phys., 10, 8821-8838, 2010.
774
775
776

Table 1: Statistical results of hourly ozone concentrations of WRF-Chem simulations (CTRL) at 1km and 4km resolution.

	11-14, May 2012				16-19, July 2015			
	CA	CA	AZ	AZ	CA	CA	AZ	AZ
	1km	4km	1km	4km	1km	4km	1km	4km
Mean Bias (ppb)	-1.9	-3.4	0.6	-0.4	-2.0	-4.0	-4.8	-4.7
Normalized Mean Bias (NMB)	-7.9	-13.5	2.5	-1.7	-8.6	-16.3	-18.5	-18.4
Normalized Mean Error (%)	16.3	25.0	15.4	16.8	24.2	34.1	24.1	25.6
Mean Normalized Bias (%)	-6.7	-10.7	3.2	-1.2	-3.5	-9.7	-16.4	-18.5
Mean Normalized Gross Error (%)	16.7	24.9	15.9	17.3	23.8	34.0	24.5	26.2
Correlation coefficient	0.75	0.54	0.76	0.65	0.74	0.4	0.75	0.61
Root Mean Square Error (ppb)	16.1	19.9	15.7	15.5	22.9	30.1	15.8	17.2

791 Captions

792 Figure 1a: 4-nested model domains--D01 to D04, from the largest rectangle box to the smallest
793 rectangle box.

794

795 Figure 1b: Innermost domain terrain elevation (m). Black dots indicate the locations of CO, NOx,
796 and/or O_3 observation sites. Circles represent surface wind observation sites. Red-dashed-line
797 box shows the southern California and black-dashed-line box stands for southern and central
798 Arizona. SGM stands for the San Gabriel Mountains; SBM indicates the San Bernardino
799 Mountains; LSBM indicates the Little San Bernardino Mountains; SJM represents the San
800 Jacinto Mountains. SGP stands for the San Gorgonio Pass, between SBM to the north and SJM
801 to the south. CP represents the Cajon Pass between SGM to the west and SBM to the east. PHX
802 stands for Phoenix metropolitan area. Lines A'A, B'B, D'D, and E'E are cross-section locations
803 and are discussed in text and Figures 8, 10, 13 and 14, respectively.

804

805 Figure 2: Surface wind comparisons between simulations (bold-red) and observations (bold
806 black). There are totally 20 sites, including those in CA and AZ with locations shown in Figure 1b
807 as circles. The variation ranges of simulation and observation are correspondently labeled by
808 thin-red-line and thin-black-line, respectively. Mean Biases (MB), RMSE and correlation
809 coefficient (R) are labeled also. CTRL represents WRF-Chem control run.

810

811 Figure 3: The comparisons of CO, NOx, and O_3 concentrations between observations (bold
812 black) and simulations (bold red) in Domain 4. There are 23 sites for NOx, 20 sites for CO, and

65 sites for O_3 observations during the study time periods. The locations are shown in Figure 1b. The variation ranges of simulation and observation are correspondently labeled by thin-red-line and thin-black-line, respectively. Missing observation time (4:00 local time) is masked in the figure. CTRL represents WRF-Chem control run.

Figure 4: Relative contributions of different emission scenarios to [O_3] at observation sites in Phoenix metropolitan area and surrounding rural areas. The dates are May 11-14, 2012 (Figure 4a-4f) and July 16-19, 2005(Figures 4g-4l). Idxxxx corresponds to the EPA AIRS site number in Maricopa County, Arizona. Black line indicates the [O_3] observation. Red line represents the simulated [O_3] for the CTRL run. Blue line shows the [O_3] for the noAZ run. Green line displays the [O_3] for the noCA run. Gray line is the [O_3] for the BILB run.

Figure 5: Simulated diurnal variations of [O_3] at Phoenix urban setting for different emission scenarios: (a) average from July 16-19, 2005, and (b) average from May 11-14, 2012.

Figure 6: Mean DMA8 [O_3] in Phoenix metropolitan area from observation (Obs), simulation from CTRL runs (CTRL), BILB runs (BILB), and the relative contributions of different emission sources. CTRL-noAZ represents the modeled DMA8 [O_3] differences between CTRL run and noAZ run. CTRL-noCA displays the modeled DMA8 [O_3] differences between CTRL run and noCA run. Observation sites show in Figure 1b. (a) DMA8 [O_3] at observation sites for July 16-19, 2005, (b) the same as (a) but for that averaged from Phoenix urban grid cells. (c) and (d), the same as (a) and (b) but for the case of May 11-14, 2012.

835

836 Figure 7: DMA8 [O_3] spatial distributions in Greater Phoenix and surround areas on July 19,
837 2005: (a) CTRL, (b), noAZ, (c) noCA, (d) BILB, (e) CTRL-noAZ, and (f) CTRL-noCA. Contours
838 represent terrain elevations. Dots show O_3 observation sites. Circle indicates the approximate
839 location of Phoenix urban area.

840

841 Figure 8: Hovmoller diagram of [O_3] differences (CTRL minus noCA) at 13th vertical model layer
842 (about 1100-m agl) along the cross-section B'B shown in Figure 1b for May case (a) and July
843 case (b). Approximate locations of Phoenix (PHX), desert, mountains (Mnts), and coast are also
844 labeled in Figure 8. The integrating is counted from 00Z, May 10, 2012, and 00Z, July 15, 2005,
845 respectively.

846

847 Figure 9: Wind vector field at 40-m above surface layer in southern California coastal area. Data
848 are averaged from 20Z to 02Z, July 16-20, 2005.

849 Figure 10: Vertical distributions of ozone along cross-section A'A (Figure 10a) and B'B (Figure
850 10b) shown in Figure 1b at 22Z of July, 17, 2005. The contours are potential temperature
851 starting at 280-K with 1-K interval.

852

853 Figure 11: Ground-level ozone concentration comparisons between observations and
854 simulations at (a) Banning Airport (ID0650012, 33.92077^o, -116.85841^o) located in the San
855 Gorgonio Pass and (b) Crestline (ID060710005, 34.24313^o,-117.2723^o) near the Cajon Pass from

July 17-19, 2005. Obs indicates the observation. CTRL represents the simulations from CTRL run and M12km is the model simulations at 12-km resolution.

Figure 12: Integrated fluxes of ozone differences (CTRL-noCA) from surface to 1400 m above ground-level: (a) average from 18Z to 02Z, July 16 to July 20, 2005, and (b) average from 03Z to 17Z, July 16 to July 20, 2005.

Figure 13: The vertical distribution of VOC (top), NOx (middle), and O_3 (bottom) along the cross-section D'D (shown in Figure 1b) in the Salton Sea Basin at 01Z, 03Z, and 06Z, July 18, 2005. Contours are potential temperature with 1-K interval.

Figure 14: The vertical distribution of VOC (top), NOx (middle), and O_3 (bottom) along the cross-section D'D (shown in Figure 1b) in the Gila River Basin, Arizona at 05Z, 11Z, and 18Z, July 18, 2005. Contours are potential temperature with 1-K interval.

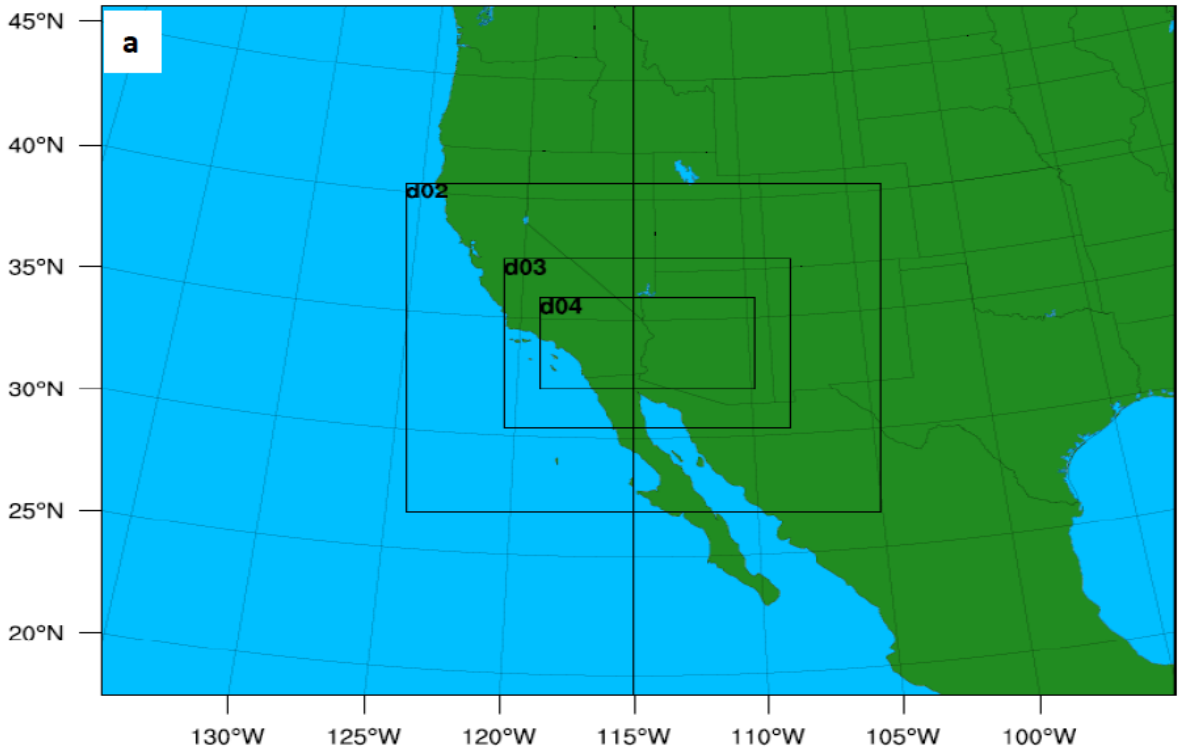

Figure 1a: 4-nested model domains--D01 to D04, from the largest rectangle box to the smallest rectangle box.

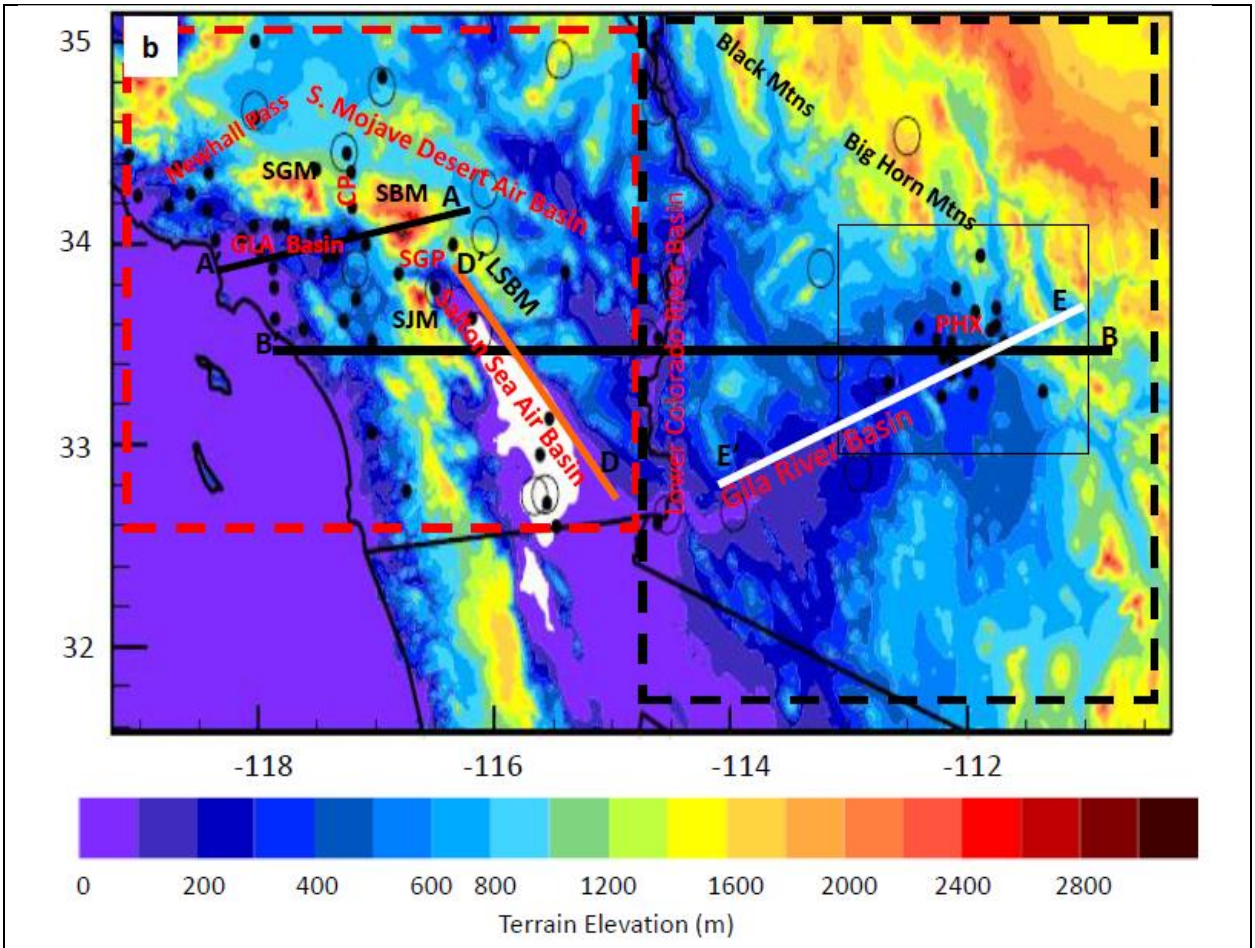

Figure 1b: Innermost domain terrain elevation (m). Black dots indicate the locations of CO, NOx, and/or O_3 observation sites. Circles represent surface wind observation sites. Red-dashed-line box shows the southern California and black-dashed-line box stands for southern and central Arizona. SGM stands for the San Gabriel Mountains; SBM indicates the San Bernardino Mountains; LSBM indicates the Little San Bernardino Mountains; SJM represents the San Jacinto Mountains. SGP stands for the San Gorgonio Pass, between SBM to the north and SJM to the south. CP represents the Cajon Pass between SGM to the west and SBM to the east. PHX stands for Phoenix metropolitan area. Lines A'A, B'B, D'D, and E'E are cross-section locations and are discussed in text and Figures 8, 10, 13 and 14, respectively.

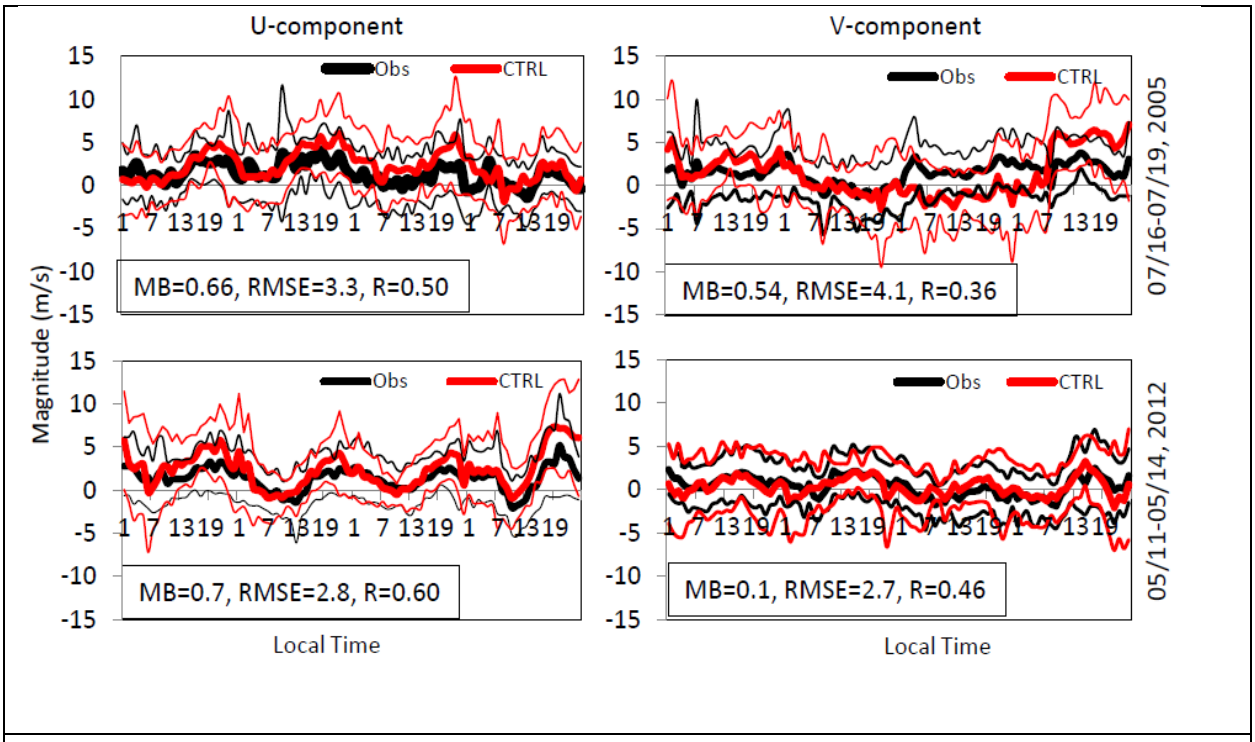

Figure 2: Surface wind comparisons between simulations (bold-red) and observations (bold black). There are totally 20 sites, including those in CA and AZ with locations shown in Figure 1b as circles. The variation ranges of simulation and observation are correspondently labeled by thin-red-line and thin-black-line, respectively. Mean Biases (MB), RMSE and correlation coefficient (R) are labeled also. CTRL represents WRF-Chem control run.

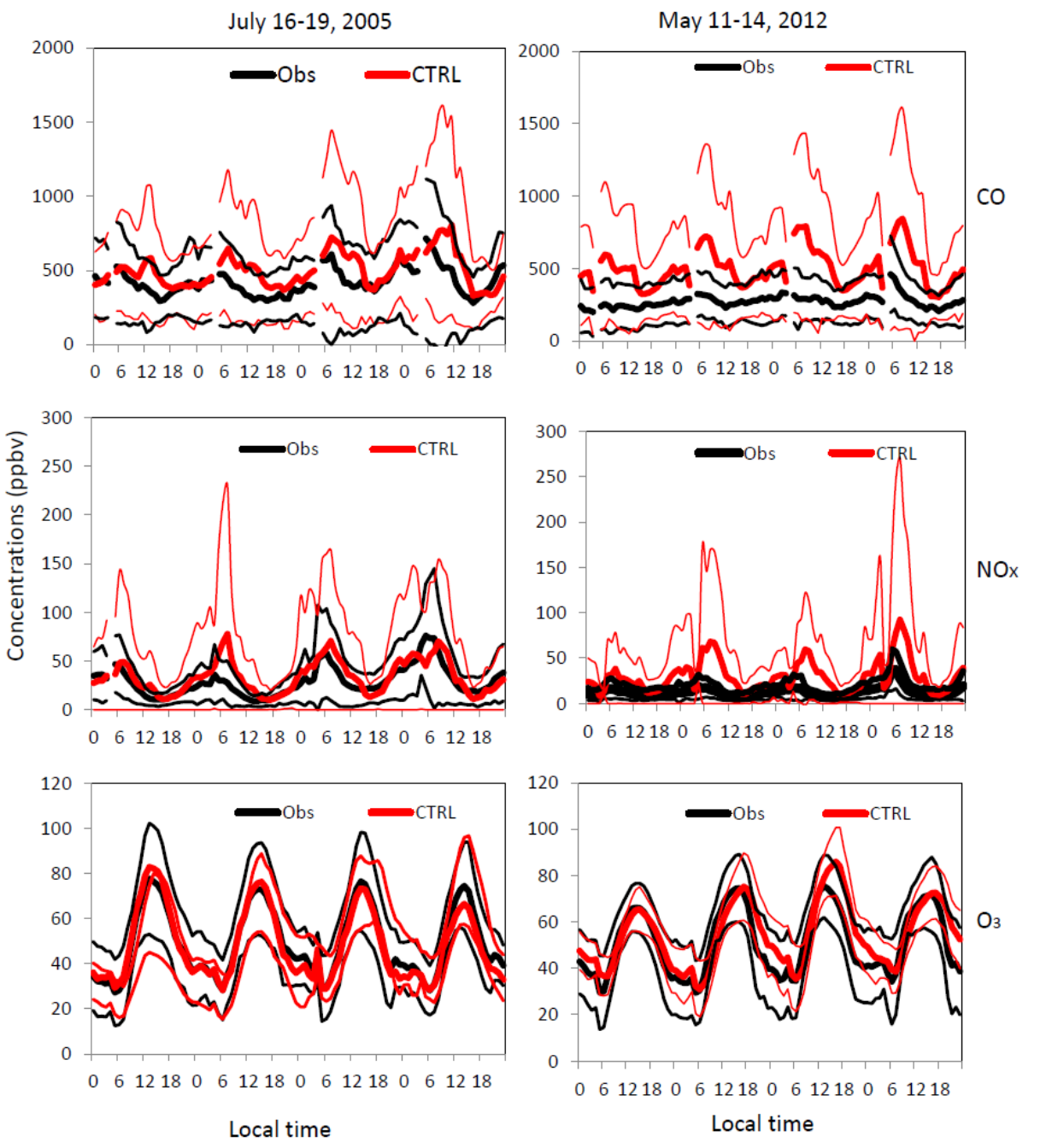

Figure 3: The comparisons of CO, NOx, and O_3 concentrations between observations (bold black) and simulations (bold red) in Domain 4. There are 23 sites for NOx, 20 sites for CO, and 65 sites for O_3 observations during the study time periods. The locations are shown in Figure 1b. The variation ranges of simulation and observation are correspondently labeled by thin-red-line and thin-black-line, respectively. Missing observation time (4:00 local time) is masked in the figure. CTRL represents WRF-Chem control run.

899

900

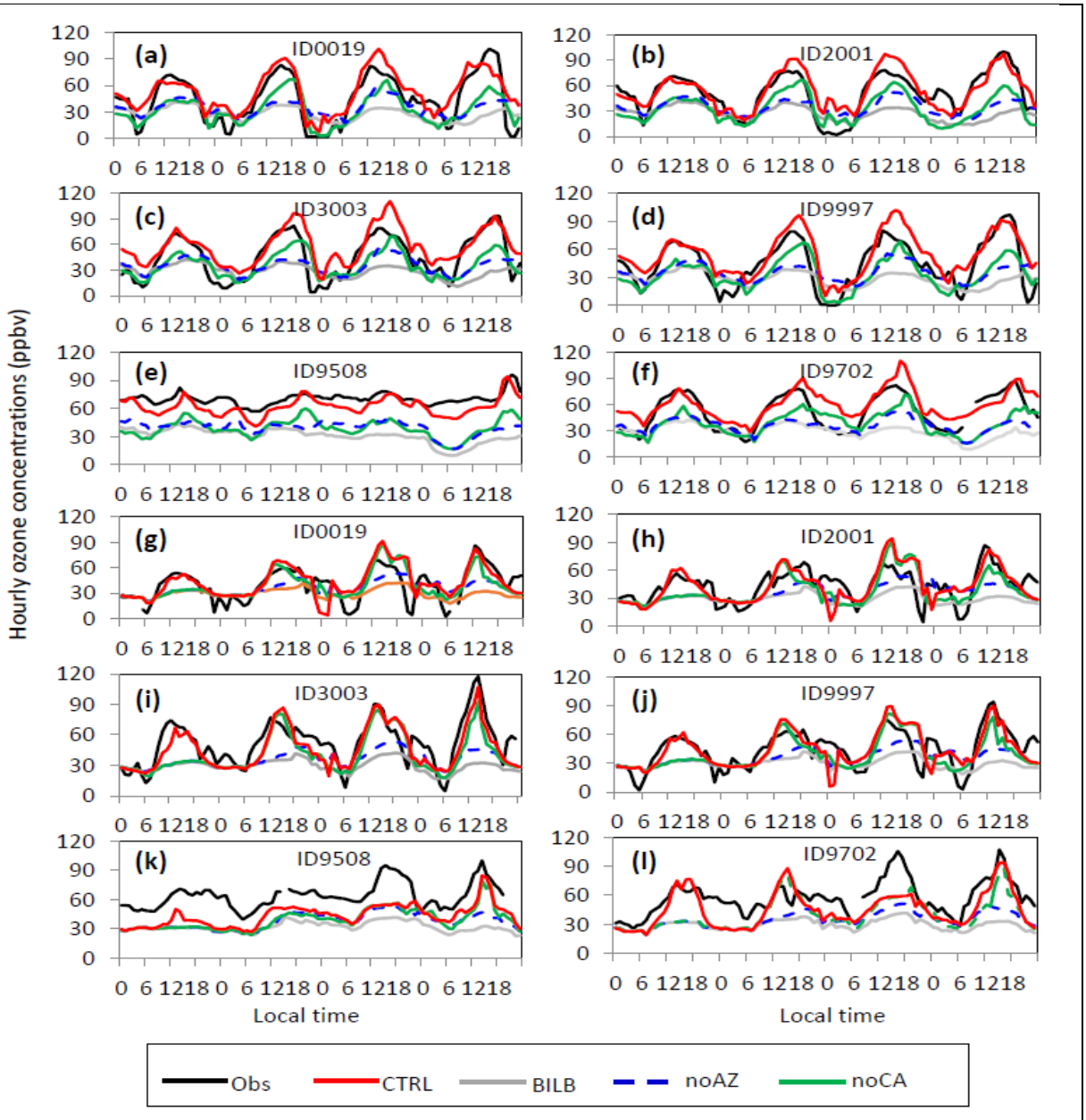

Figure 4: Relative contributions of different emission scenarios to [O_3] at observation sites in Phoenix metropolitan area and surrounding rural areas. The dates are May 11-14, 2012 (Figure 4a-4f) and July 16-19, 2005(Figures 4g-4l). Idxxxx corresponds to the EPA AIRS site number in Maricopa County, Arizona. Black line indicates the [O_3] observation. Red line represents the simulated [O_3] for the CTRL run. Blue line shows the [O_3] for the noAZ run. Green line displays the [O_3] for the noCA run. Gray line is the [O_3] for the BILB run.

901

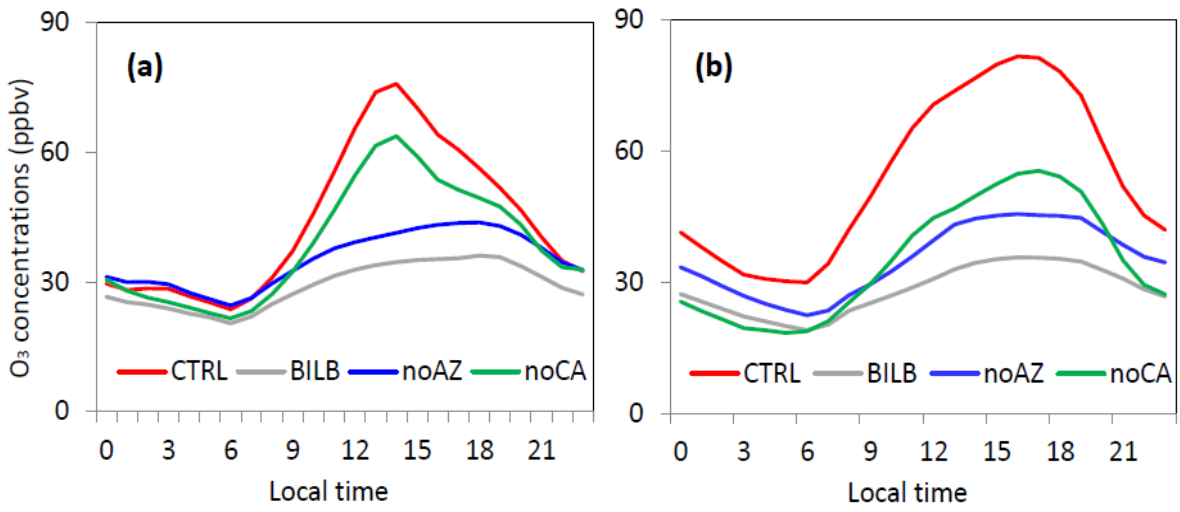

Figure 5: Simulated diurnal variations of [O_3] at Phoenix urban setting for different emission scenarios: (a) average from July 16-19, 2005, and (b) average from May 11-14, 2012.

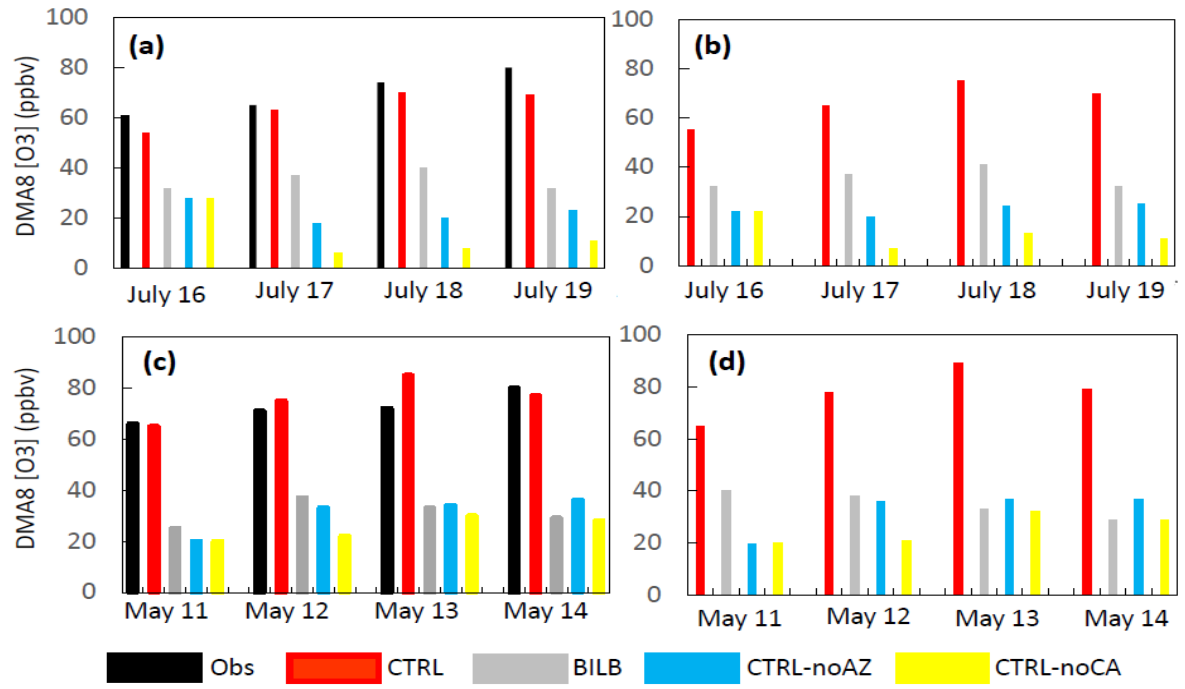

Figure 6: Mean DMA8 [O_3] in Phoenix metropolitan area from observation (Obs), simulation from CTRL runs (CTRL), BILB runs (BILB), and the relative contributions of different emission sources. CTRL-noAZ represents the modeled DMA8 [O_3] differences between CTRL run and noAZ run. CTRL-noCA displays the modeled DMA8 [O_3] differences between CTRL run and noCA run. Observation sites show in Figure 1b. (a) DMA8 [O_3] at observation sites for July 16-19, 2005, (b) the same as (a) but for that averaged from Phoenix urban grid cells. (c) and (d), the same as (a) and (b) but for the case of May 11-14, 2012.

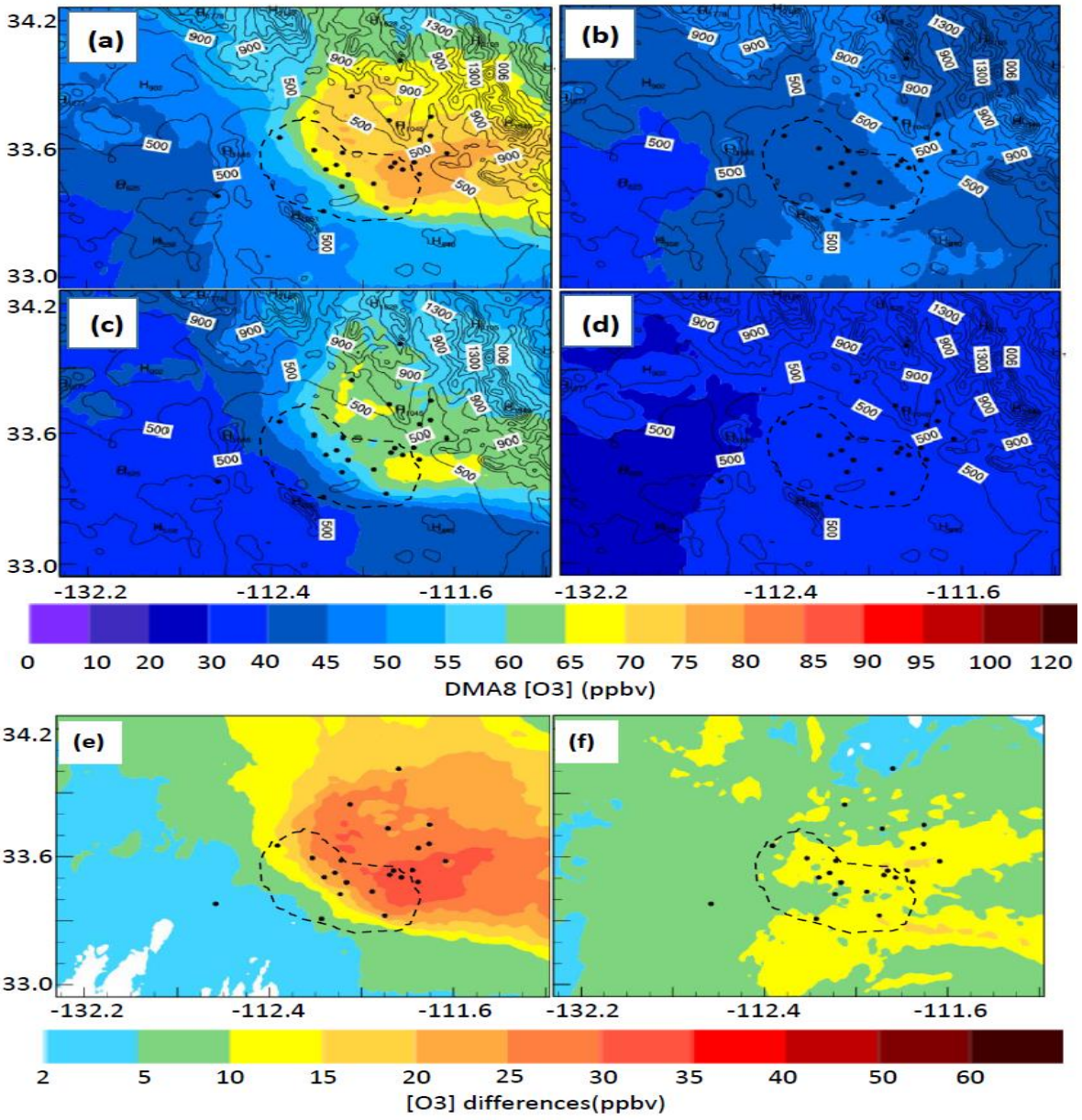

Figure 7: DMA8 [O_3] spatial distributions in Greater Phoenix and surround areas on July 19, 2005: (a) CTRL, (b), noAZ, (c) noCA, (d) BILB, (e) CTRL-noAZ, and (f) CTRL-noCA. Contours represent terrain elevations. Dots show O3 observation sites. Circle indicates the approximate location of Phoenix urban area.

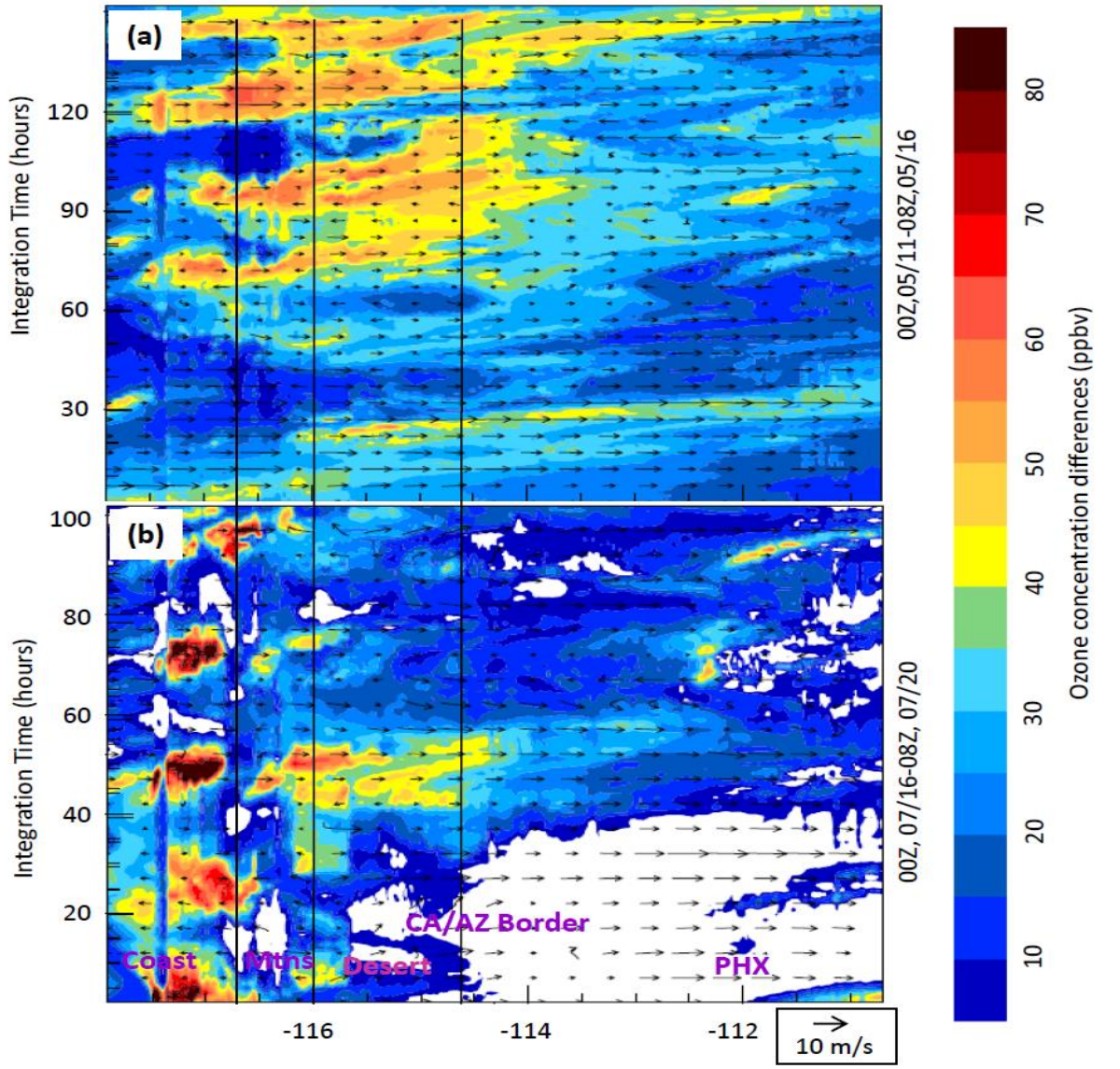

Figure 8: Hovmoller diagram of [O_3] differences (CTRL minus noCA) at 13th vertical model layer (about 1100-m agl) along the cross-section B'B shown in Figure 1b for July case (top) and May case (bottom). Approximate locations of Phoenix (PHX), desert, mountains (Mnts), and coast are also labeled in Figure 8. The integrating is counted from 00Z, May 10, 2012, and 00Z, July 15, 2005, respectively.

922

923

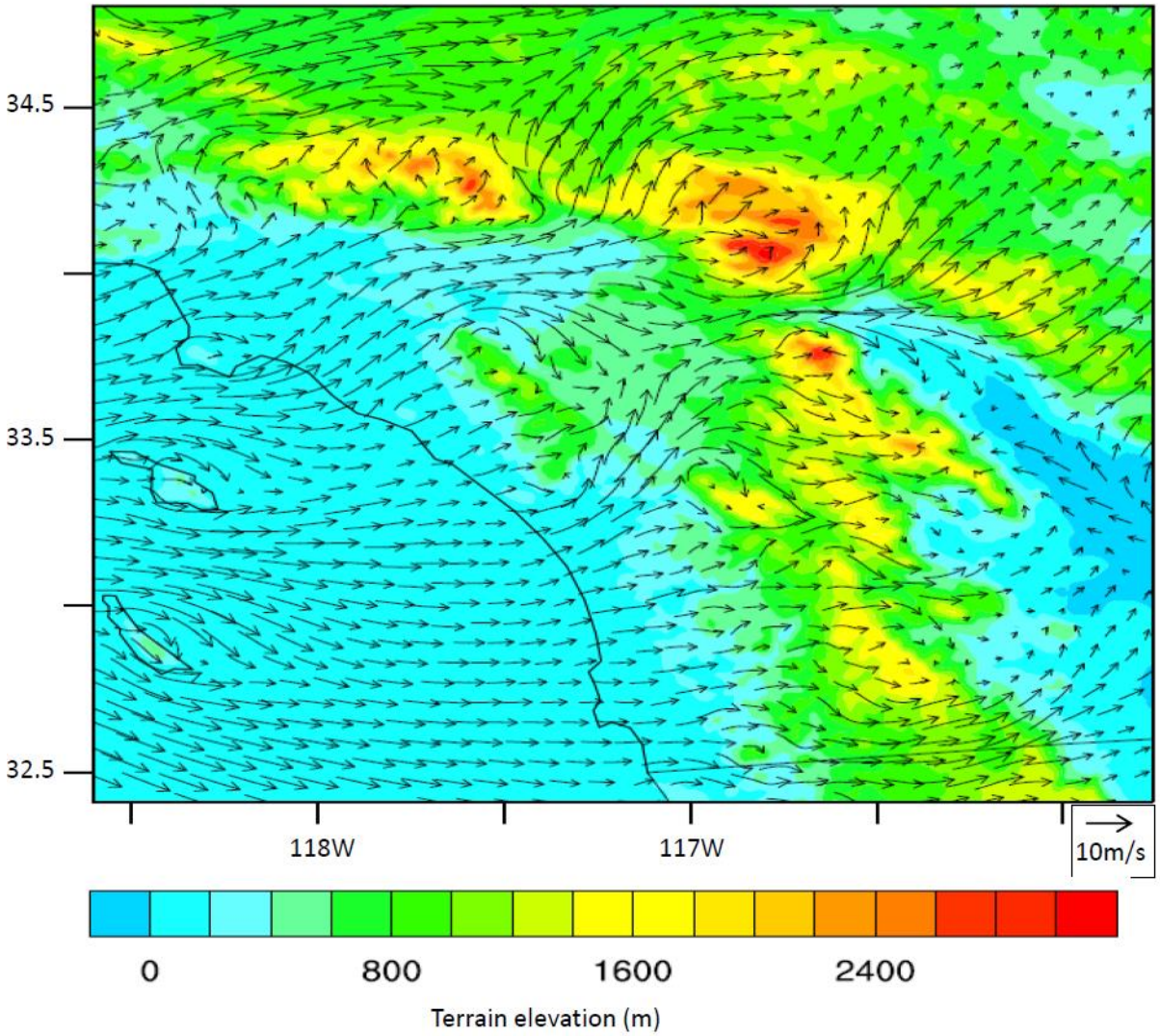

Figure 9: Wind vector field at 40-m above surface layer in southern California coastal area.

Data are averaged from 20Z to 02Z, July 16-20, 2005.

924

925

926

927

928

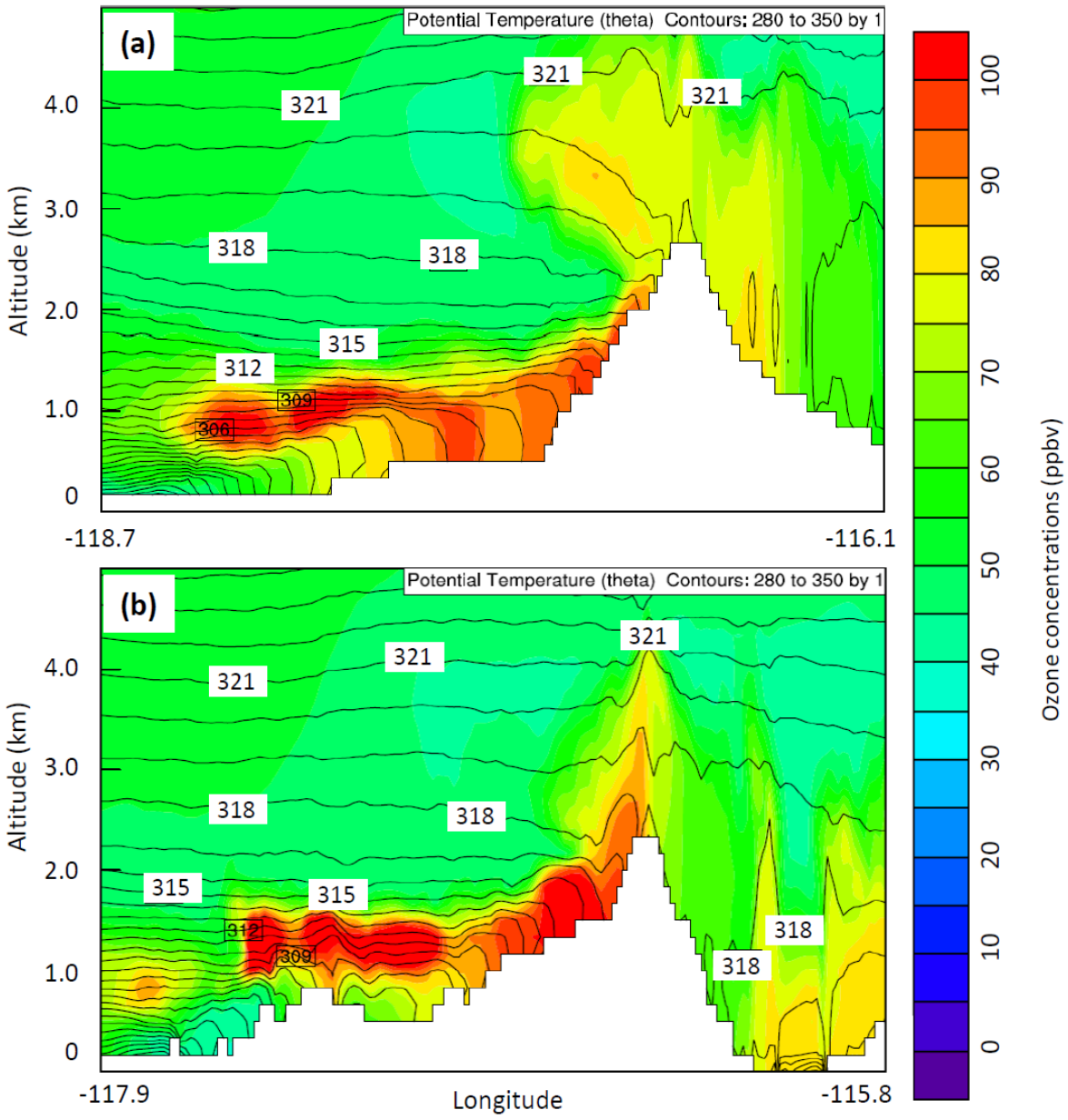

Figure 10: Vertical distributions of ozone along cross-section A'A (Figure 10a) and B'B (Figure 10b) shown in Figure 1b at 22Z of July, 17, 2005. The contours are potential temperature starting at 280-K with 1-K interval.

929

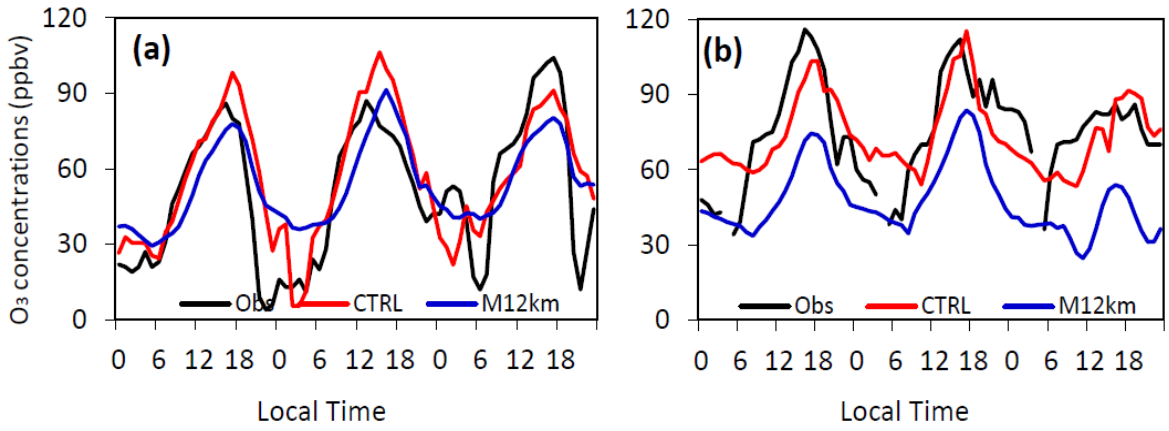

Figure 11: Ground-level ozone concentration comparisons between observations and simulations at (a) Banning Airport (ID0650012, 33.92077°, -116.85841°) located in the San Gorgonio Pass and (b) Crestline (ID060710005, 34.24313°,-117.2723°) near the Cajon Pass from July 17-19, 2005. Obs indicates the observation. CTRL represents the simulations from CTRL run and M12km is the model simulations at 12-km resolution.

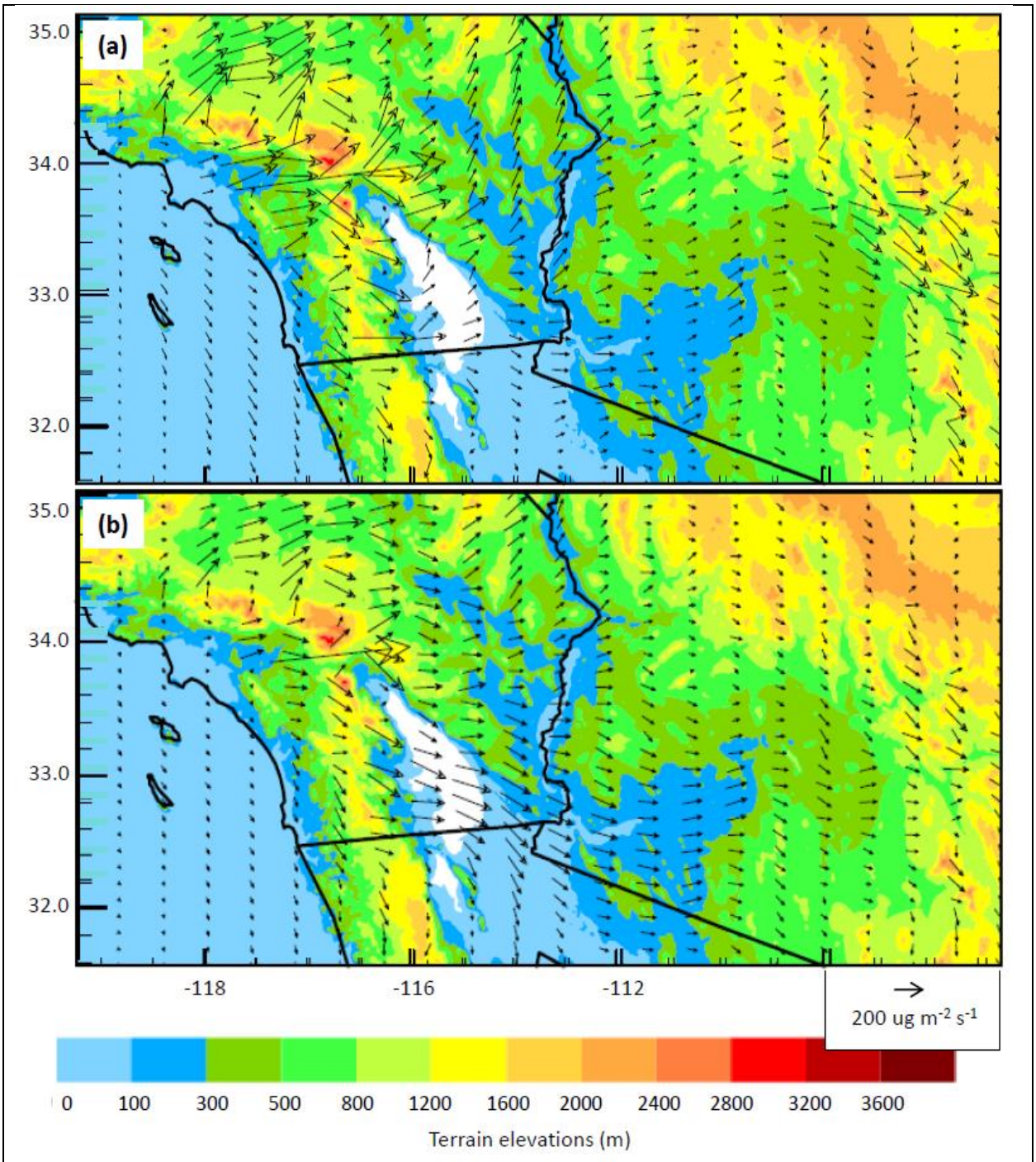

Figure 12: Integrated fluxes of ozone differences (CTRL-noCA) from surface to 1400 m above ground-level: (a) average from 18Z to 02Z, July 16 to July 20, 2005, and (b) average from 03Z to 17Z, July 16 to July 20, 2005.

941

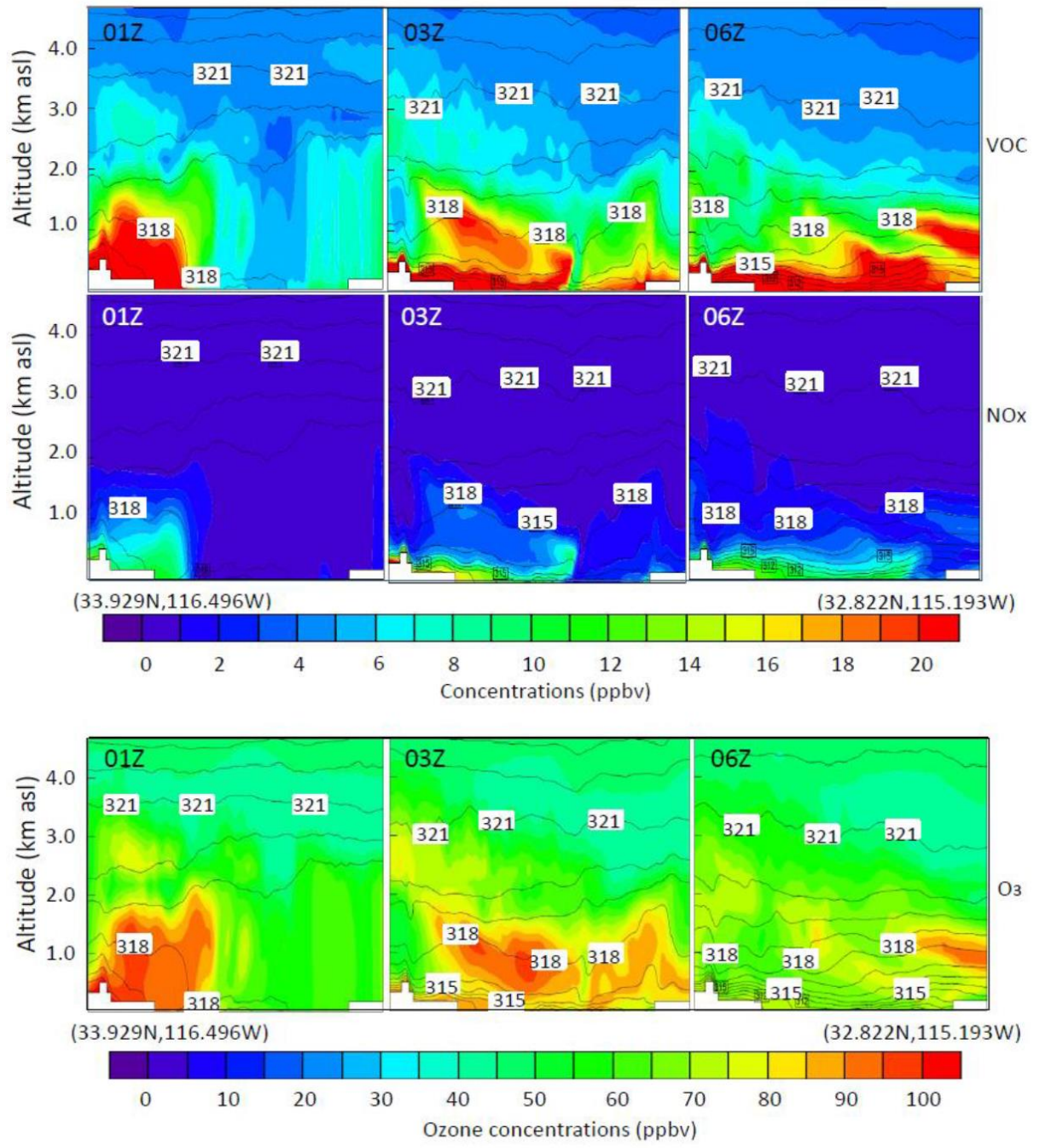

Figure 13: The vertical distribution of VOC (top), NOx (middle), and O_3 (bottom) along the cross-section D'D (shown in Figure 1b) in Salton Sea Basin at 01Z, 03Z, and 06Z, July 18, 2005. Contours are potential temperature with 1-K interval.

942

943

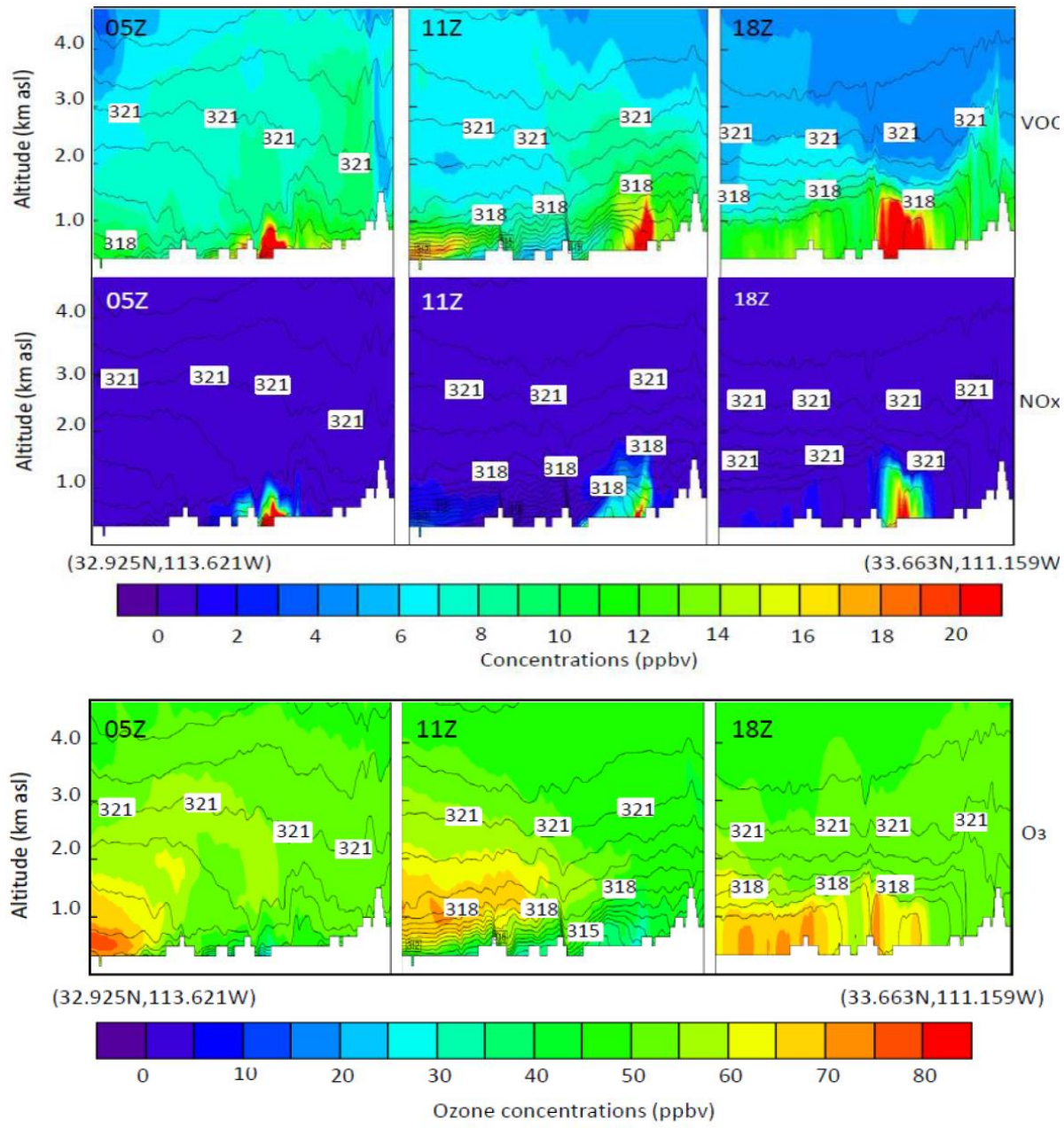

Figure 14: The vertical distribution of VOC (top), NOx (middle), and O_3 (bottom) along the cross-section D'D (shown in Figure 1b) in Gila River Basin, Arizona at 05Z, 11Z, and 18Z, July 18, 2005. Contours are potential temperature with 1-K interval.

944